Chemical Engineering Science 321 (2026) 122797

Contents lists available at ScienceDirect

Chemical Engineering Science

journal homepage: www.elsevier.com/locate/ces

2D lattice-boltzmann method with detailed surface chemistry: conservation of geometrical surface

Matthias Hettel [a,*], Eric A. Daymo [b], Nilesh Sawant [c], Olaf Deutschmann [a]

[a] Institute for Chemical Technology and Polymer Chemistry, Karlsruhe Institute of Technology (KIT), Engesserstraße 20, Karlsruhe 76131, Germany
[b] Tonkomo, LLC, Gilbert, AZ 85297, United States
[c] ETH Zurich, Department of Mechanical and Process Engineering, Zurich 8092, Switzerland

ARTICLE INFO

Keywords:
Lattice-boltzmann method
D2Q9
Catalysis
Detailed surface chemistry
Microkinetics model
Geometrical surface
Formaldehyde conversion CH_2O

ABSTRACT

The paper discusses the coupling of detailed surface chemistry to the Lattice-Boltzmann Method and shows an approach on how the geometrical catalytic surface can be preserved.

Results from calculations with the 2D LBM code MATRICS for formaldehyde conversion in a channel show good agreement compared to measurements under diffusion-controlled conditions, but not for a kinetically controlled system. Results fit for both modes of operation with results from a Finite-Volume code.

Modeling of systems with surface chemistry requires the consideration of the exact geometrical surface. However, basis of LBM is a staircase approximation for interfaces between fluid and solid. Based on theoretical derivations, it was shown that the asymptotic discretization error for circles is 27%. The error of skew lines is maximal for an angle of $\alpha = 45°$ and shows the value of 41%. The discretization error for curvilinear interfaces cannot be diminished by grid refinement.

An approach was developed, which allows the use of the exact geometric surface for calculation of surface chemistry. It consists of two steps: 1. Implementation of the species fluxes at surfaces as volumetric sources in wall bounded fluid cells. 2. Segmentation of the original geometrical surface and assignment of line segments to reactive wall cells located nearby.

The validation of the approach by calculation of flows around circles and rotated squares shows the discretization errors predicted by theory and allows to suppress the errors due to the incorporation of the exact size of curvilinear or skew geometrical interfaces in the calculation.

1. Introduction

1.1. Lattice Boltzmann method

Lattice Boltzmann methods can be interpreted as discrete solution procedures of the Boltzmann equation or its approximation, the BGK (Bhatnagar Gross Krook) model. The methods are based on an equally discretized space (lattices) under the assumption of near-continuum flow with *Knudsen number* $= l_{free}/L \ll 1$, where the mean free path length l_{free} is replaced by the spatial step size δx, and L is a typical macroscopic length of the problem under consideration. It can be shown that the *standard* LBM is a second-order accurate solver for the weakly compressible Navier-Stokes equation. The *weak compressibility* refers to errors that become relevant as $Ma \to 1$ (Krüger et al., 2017).

The LBM is a relatively young method and is still evolving at a rapid pace, meaning that the range of problems to which it can be effectively applied is still increasing (e.g. turbulence, multi-phase systems, multi-component fluids, micro scale flows, flows through porous media, quantum mechanics, etc.). A field of application which is addressed only sparsely so far is the calculation of flows in combination with detailed homogeneous chemistry or heterogeneous surface chemistry at fluid–solid interfaces. Calculating flows with reactions usually implies that the density is variable. This is a challenge for developing new models for LBM, as classical LBM models are based on the presumption of constant density. However, there are also many applications that involve chemistry where the density remains constant as a first approximation.

* Corresponding author at: Matthias Hettel, Institute for Chemical Technology and Polymer Chemistry, Karlsruhe Institute of Technology (KIT), Karlsruhe 76128, Germany.
E-mail address: matthias.hettel@kit.edu (M. Hettel).

https://doi.org/10.1016/j.ces.2025.122797
Received 29 August 2025; Received in revised form 2 October 2025; Accepted 14 October 2025
Available online 17 October 2025

1.2. LBM and chemistry

The article by Hosseini (Hosseini et al., 2024) gives an overview of LBM for combustion applications. However, in the following, we will primarily concentrate on works related to heterogeneous chemistry.

Khang (Kang et al., 2014) developed a multi-component thermal model for catalytic systems. For every species a different grid is needed. To overcome this issue, the authors propose setting the grid size to that needed for the lightest species in the system, and for other species to use interpolation in order to reconstruct distribution functions on the grid. Results of D2Q9 calculations of a channel with reactive walls for a one-step global reaction show good agreement with results from a Finite-Volume Method (FVM) solver.

Further development of the model resulted in the work of Khatoonabadi (Khatoonabadi et al., 2024). Three-dimensional Lattice Boltzmann (LB) simulations were carried out to investigate the mass transport and reaction inside and around catalytic porous particles used in fluidized beds for the synthesis of methane from biogas, based on a one-step reaction. The 3D internal porous structure of a real particle with a size ~200 μm was available. Pore-resolved calculations reveal the influence of different diffusion coefficients for species on the overall conversion. The important question of how the real internal surface is reproduced by the lattice grid is not addressed.

The modeling of flow and catalytic reaction in resolved washcoats can be found in the paper by Belot (Belot et al., 2021). Sections of catalyzed filter walls, with varying amounts of washcoat and different levels of uniformity, were digitally reconstructed from tomography data. The calculations were performed in 3D. Constant density was assumed, as the concentrations were small. Based on solution of flow field, the catalytic conversion (one step chemistry) and mass transport of a hypothetical dilute species was solved. The problem of how the surface of each lattice is handled is not discussed. However, it is mentioned that the voxelized surface is too large. Therefore, a correction parameter of 1.5 has been introduced.

Sawant et al. (Sawant et al., 2021; Sawant et al., 2022) propose a LBM for compressible reacting multi-species flows recovering the Stefan–Maxwell diffusion closure. The model uses $N_{sp} + 1$ LB equations: a population for the mixture-averaged mass and momentum balance, a population for the mixture-averaged energy balance and $N_{sp} - 1$ populations for N_{sp} species. This model, in combination with compressible LBM for momentum and energy balance equations, has been successfully used for a variety of cases involving combustion applications with detailed chemistry (e. g. periodic ignition and extinction in a channel, circular expanding premixed flame). The D3Q27 lattice code is coupled to the open source code chemical kinetics solver Cantera (Goodwin et al., 2024).

Filippova (Filippova and Hänel, 2000) discusses an extended Lattice Boltzmann model for the simulation of low Mach number flows with significant density changes. For applications to reactive flows, this model was coupled with a finite-difference scheme for solving the transport equations of energy and species. The model was applied to calculate the flow of a hot oxidizer around a cylinder. Through the surface, cold fuel is injected into the flow and reacts via a one-step global reaction. The boundary condition used is discussed later in this section.

In the work from Arcidiacono (Arcidiacono et al., 2008) a multi-component LB model is discussed. The equilibrium distribution functions were obtained by maximizing the entropy function. The quasi-equilibrium distribution functions were deduced by assuming that, in the multicomponent mixture, particular moments approach equilibrium slower than others. Results of calculations of a straight channel based on D2Q9 lattice including a four-component mixture and a global catalytic methane oxidation are in excellent agreement with a FVM solver in terms of both the flow field and species concentrations.

Succi (Succi et al., 2002) calculated a quasi-incompressible, isothermal flow with species transport and catalytic chemical reactions. The flow field is solved by a Lattice Boltzmann method, while the multi-species transport and chemical reactions are handled with a variant of the Lax–Wendroff method. Small obstacles were placed in a microchannel and due to influence on the flow field, led to an increase in overall conversion of pollutants based on a one-step chemistry. The reaction takes place on flat channel walls.

From Lee (Li et al., 2013) is a work where the catalytic reaction in resolved porous media was calculated. Fractal theory was applied to create two dimensional square shaped structures (no curvilinear or inclined surfaces). A D2Q9 lattice BGK model was used to solve for the flow, temperature and concentration fields. Chemistry was a one-step dehydrogenation of isopropanol. The influence of temperature on velocity was neglected. The effect of the chemical reaction on the velocity field was considered by adding a velocity component normal to reactive surfaces, combined with the change of the mixture density.

1.3. Boundary conditions for surface chemistry

In classical CFD (Computational Fluid Dynamics) approaches such as FVM (Finite Volume Method) or FEM (Finite Element Method) often the mean-field approach is the method of choice for the modelling of surface chemistry. Therein, the local state of the surface is described by its coverage with adsorbed species, averaged on a microscopic scale. It is assumed that models exist that can compute the local heterogeneous reaction rate as a function of the local conditions such as temperature and species concentration in the gas-phase and of the local and temporal state of the surfaces. Chemical source terms of the gaseous species taking part in surface chemistry are delivered in the unit [kmol/m^2/s]. To incorporate the chemical source terms in the species transport equations these have to be multiplied by the geometrical surface of a catalyst. Therefore, it is essential that the size of geometrical surface is conserved in the model.

When applying FVM or FEM, a variety of cell shapes exist for the definition of the computational grid. Any geometrical surfaces or interfaces between fluid and solid can be discretized with body fitted elements. Doing so, the deviation between real and discretized surface is in general small for practicable grid resolutions. An important feature is, that this deviation decreases with grid resolution. The boundary treatment itself is trivial.

Boundary conditions in Lattice-Boltzmann models are fundamentally different from their equivalents for more traditional computational fluid dynamics methods. The populations entering the domain have to be defined, even if the boundary is an inert solid wall. In general, the number of macroscopic conditions on the boundary is insufficient to calculate all incoming populations. Additionally, great care has to be taken in the development of boundary conditions in order to obtain stable simulations (Ginzburg and d'Humières, 2003).

In LBM all cells have the same size and a square shape. A cell as a whole can belong either only to fluid or to solid domain. The surfaces of the cells, and therefore, also the interfaces between fluid and solid, are oriented straight horizontally or vertically. This means, that curvilinear or skew geometrical boundaries are commonly replaced by staircase-shaped boundaries. In LBM codes the usage of staircase-shaped interfaces is standard because this is the easiest way and leads to satisfactory results for many applications. One method of discretizing curved boundaries with the staircase-shaped interfaces is the Simple Bounce Back (SBB) method (Krüger et al., 2017). An intrinsic characteristic is, that the deviation between staircase-shaped interface and real interface does not decrease with resolution, as will be proven later. With respect to boundary treatment there are special procedures available to account for complex geometrical shapes. In the end, all of these procedures lead to interpolation and extrapolation of populations.

With respect to the actual work, fluid–solid interfaces are stationary and do not move or deform in time which simplifies the problem. There exists a wide range of boundary conditions for curved interfaces for LB simulations (Krüger et al., 2017), some of which are reviewed below.

The Interpolated Bounce Back (IBB) method is a common extension

of the simple bounce back (SBB) (Bouzidi et al., 2001). It is assumed that any population f_i moves a distance of one cell size δx during propagation. If the population hits a wall which is modelled by the halfway bounce-back, f_i first travels a distance $\delta x/2$ from the original boundary node to the wall and, after bounce-back, the same distance back to the boundary node. As curvilinear walls are not located halfway between lattice nodes, f_i cannot reach another lattice node. Therefore, the origin of the population is chosen such that f_i exactly reaches a lattice node. This requires interpolation to find the post-collision values of f_i.

Central part of the family of Partially Saturated Methods (PSM) is a modified BGK equation (Noble and Torczynski, 1998). A lattice node can be a pure fluid, a pure solid or a mixed (partially saturated) node. Based on the solid fraction ε of each node a weighting parameter, B, is defined which is used to modify the standard BGK collision operator. In reality, curved boundaries in the PSM are nothing more than a sophisticated staircase. In the PSM, there is no information about the distance between lattice nodes and boundaries; instead, the local solid fraction ε is considered. It is easy to imagine that many different boundary configurations can lead to the same filling fraction. Therefore, the PSM sometimes fails to capture the correct shape of the boundary (Krüger et al., 2017).

Another class of approaches are the so-called *ghost methods*. The original formulation was proposed by Filippova (Filippova and Hänel, 1998). It allows the description of Dirichlet boundary conditions for velocity on arbitrary curvilinear surfaces lying between the nodes of a Cartesian grid. The distribution functions in the cells next to the wall are modified by the prescribed flux. The method was used to model species fluxes coming out of a porous wall. This requires extrapolation of the wall flux to the cell next to the wall. Both the BGK equation and the equilibrium populations f_i^{eq} are modified. An adjustment parameter must be introduced to guarantee the stability of the system.

Falcucci (Falcucci, 2020) shows in his very interesting work the application of isothermal LBM to catalytic reactors as well as to microbial fuel cells. The one-step oxidation of methanol to methyl formate in a porous ingot with gold nanoparticles as catalyst was investigated. The random nano-porous substrate was virtually constructed. The ingot was placed perpendicular to a flow field. The 2D results indicate that the catalyst layer on the ingot side facing the gas stream shows a high conversion efficiency, in contrast to the rear face of the ingot. The overall conversion efficiency gets dramatically reduced if the ingot is oriented parallel to flow. Additional 3D calculations were performed for one-step NO reduction in a channel of a monolith. Both the channel and the washcoat were resolved. For the implementation of single-step surface chemistry a special (*coast-line sputtering*) boundary was developed which also accessed *ghost nodes*. The results deliver accurate and reliable predictions. The question about size of catalytic surface was not discussed.

Approaches which are well known in FVM CFD can be transferred into the LBM framework. One method is the Level Set Method applied in the work by Yoshida (Yoshida and Nagaoka, 2010). He proposes a LBM for the convection–diffusion equation, which is able to cover the anisotropic diffusion-coefficient tensor. The approach was tested for a 2D flow around a sphere, where the boundary line was given by a mathematical function and shows agreement to FVM results.

Another approach is the Volume-of-Fluid Method used in the paper by Verhaege (Verhaeghe et al., 2006). It works with a volume fraction of solid in every boundary cell. From this, a virtual dimensionless distance to the interface can be constructed, and via ghost nodes and interpolation, the flux normal to surface can be reconstructed. However, the geometrical interface is not known or cannot be exactly conserved.

Nearly all the methods mentioned for handling curved surfaces are developed for the calculation of the flow field near walls and improve the prediction of forces and wall shear stresses. All these methods lack the explicit use of the exact surface of geometries including skew or curvilinear walls. Also, to the best knowledge of the authors, no work exists that discusses the combination of detailed surface chemistry and curvilinear surfaces, where the surface size is exactly conserved.

The nature and the error in using staircase-shaped interfaces will be shown both for circles and inclined walls. An approach is developed to incorporate the exact geometrical surface in the calculations. In the following, this approach will be labeled as ESC (Exact Surface Conservation) method.

2. Methods

In this section the computational methods used for the present study are introduced, including an introduction to the Mean-field-approach.

2.1. CFD and heterogeneous microkinetics

2.1.1. Mean-Field approach

The description of surface reactions is analogous to that of gas-phase reactions. However, since there exist almost innumerable numbers of different surface structures, only little is known about the exact reaction paths. Instead of looking at interactions between single adsorbed species, the mean-field approximation is a common choice for modeling (Kee et al., 2003; Deutschmann, 2011).

Within the framework of the mean-field approximation the calculation of the total molar production rate $\dot{s}_a$ of a gaseous species or an adsorbed surface species a (in [kmol/m^2/s]) is calculated as a product of rate coefficients and concentrations c_a determined by:

$$\dot{s}_a = \sum_{k=1}^{K_s} \nu_{ak} k_k \prod_{a=1}^{N_g+N_s+N_b} C_a^{\nu_{ak}} \qquad (a = 1, \cdots, N_g + N_s + N_b). \tag{1}$$

Here, K_s is the number of surface reactions (including adsorption and desorption) among N_g gas-phase, N_s surface and N_b bulk species (species for which no conservation equation is solved). ν_{ak} are the stoichiometric coefficients, C_a are the concentrations of the species, and k_k are the forward rate coefficients described by an Arrhenius expression.

Most catalysts exhibit a certain structure, for instance, they may occur as dispersed particles on a flat (Fig. 1 left) or in a porous (Fig. 1 right) substrate. Examples are thin catalytically coated walls in honeycomb structures, foams, disks, plates, and well-defined porous media (e.g. particles). An example is a washcoat, which is a thin layer of supporting material where small particles of the catalytic active material (e.g. precious metals) is embedded in a supporting material. The numerical grid resolves only the flow region bounded by the geometrical structure of the catalyst (green outlines in Fig. 2). The simplest way to account for the active catalytic surface area consists in calculating the flux $\dot{R}_a$ (in [kmol/s]) of a specie a at the interface between fluid) in the following form:

$$\dot{R}_a = A_{interface} \bullet F_{cat/geo} \bullet \dot{s}_a \tag{2}$$

Here, $\dot{s}_a$ is the molar net production rate of gas phase species a, given in [kmol/m^2/s]. The area $A_{interface}$ refers to the actual *catalytically active surface area* (red outlines in Fig. 1). The parameter $F_{cat/geo}$ represents the amount of *catalytically active surface area* in relation to the *geometric surface area* (green outlines in Fig. 1) of the fluid–solid interphase. Depending on porosity of the support and the dispersion (e.g. of particles of precious metals) this factor can range from one up to the order of hundred. The *catalytically active surface area* is the surface area of the catalytic active particles exposed to the ambient gas (fluid) phase. This area can be determined experimentally. The *catalytically active surface area* should not be confused with the BET (Brunauer-Emmett-Teller) surface area representing the *total inner surface area* of a porous structure (blue outline in Fig. 1 right) (see also (Hettel et al., 2018).

The effectiveness factor η_i represents the ratio of the reaction rate to the rate which would occur without internal diffusion limitations inside porous solids (washcoats, particles). This factor includes the following

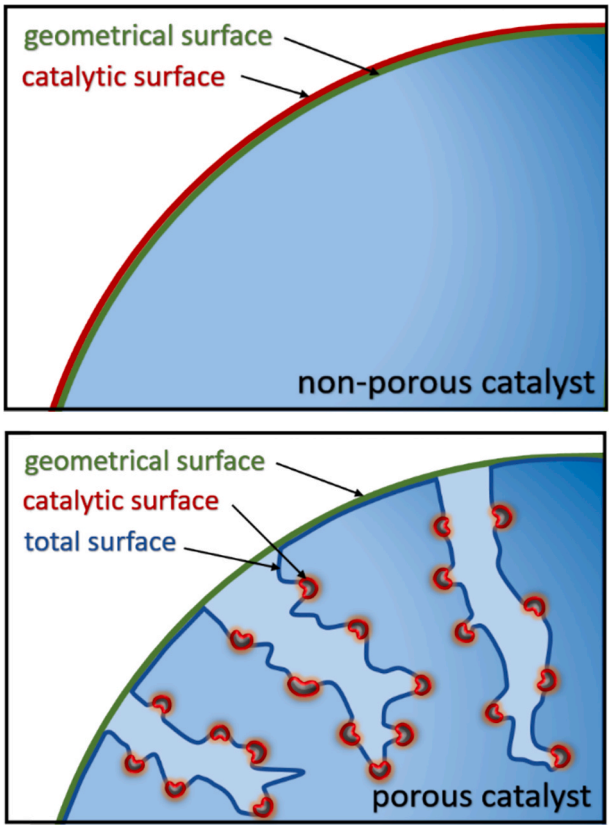

Fig. 1. Top: Definition of surface areas for a non-porous catalyst. Bottom: Definition of surface areas for porous catalysts (or porous layers such as washcoats).

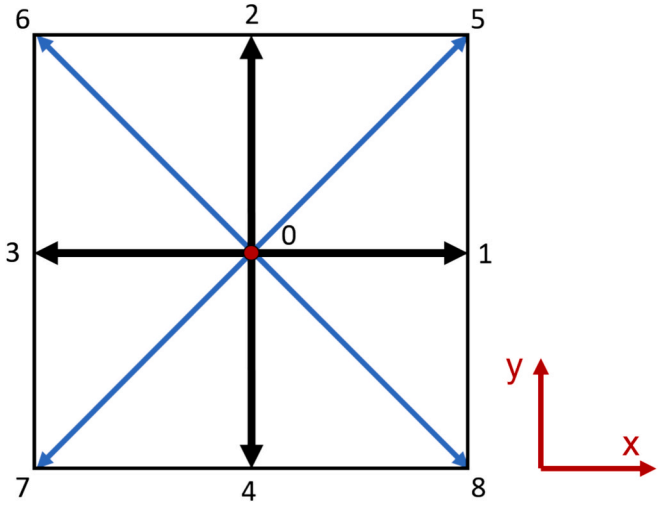

Fig. 2. The D2Q9 lattice with velocities $|c_i| = 1$ and $\sqrt{2}$ are shown in black and blue, respectively. Rest velocity is $c_0 = 0$. The square has an edge length of $2\delta x$.

parameters: concentration of the species at the boundary between fluid and washcoat, washcoat thickness and effective diffusion coefficient in a porous substrate (Deutschmann, 2011). The product $(F_{cat/geo} \bullet \eta_i)$ is used in the actual work to simultaneously account for active catalytic surface area and internal diffusion limitation and is represented by the term only $F_{cat/geo}$ in subsequent sections.

2.1.2. Microkinetic model for oxidation of formaldehyde

The global reaction scheme for the catalytic oxidation of CH_2O (formaldehyde) over Pt is given as

$$CH_2O + O_2 \xrightarrow{Pt(s)} H_2O + CO_2 \quad (3)$$

In this work a thermodynamically consistent multi-step surface reaction mechanism is used (Torkashvand et al., 2019). The mechanism contains 6 gas-phase species (N_2, O_2, H_2, H_2O, CO, CO_2, CH_2O), 10 surface species (Pt(s), H(s), O(s), H_2O(s), CO_2(s), CO(s), CH_2O(s), OH(s), C(s), HCO(s)) and 30 elementary steps. With respect to reaction path CH_2O from the gas-phase is first adsorbed on the empty platinum site as HCHO(s), and dehydrogenated to HCO(s) and further to CO(s) by O(s) or Pt(s), and finally oxidized to CO_2(s).

Since no gas-phase reactions can be detected under the conditions in this study, no gas-phase reaction mechanism is included.

2.1.3. Generic simple reaction model

To keep things simple the calculations for the investigation of the approach to use the exact geometrical surface a generic kinetic model was used. Species A is converted to species B via the reaction scheme:

$$A + Pt(s) \xrightarrow{Pt(s)} B + Pt(s) \quad (4)$$

$Pt(s)$ is a free surface place of the actice catalyst material platinum. The rate coefficient was chosen to be $r = 1{\cdot}10^{-4}$ [1/s].

2.2. 3D FVM code DUO

For the validation of the results from the code MATRICS, we used the tool DUO, which stands for the coupling of the two computer codes DETCHEM Und (German for 'and') OpenFOAM and is a synonym for the joint utilization of these two programs.

OpenFOAM OpenFOAM-The Open Source CFD Toolbox is an open source CFD tool, which enables the calculation of multiple combined three-dimensional fluid and solid regions. It is based on the Finite-Volume Method (FVM). By being open-source, OpenFOAM offers users complete freedom to customize and extend its existing functionality. However, the consideration of surface reactions is not possible.

Therefore, the DETCHEM™ code was combined to OpenFOAM. DETCHEM^{TM} (Deutschmann et al., 2014) is a commercially available package of tools specifically designed for the modeling and simulation of reacting flows based on elementary step mechanisms, particularly for heterogeneous systems such as catalysis, materials synthesis and fuel cells. The basic idea is to combine the advantages of the two programs. The simulation tool DUO is the gateway between the two codes (Hettel et al., 2015; Hettel et al., 2018).

A precompiled shared library (programmed in Fortran 90), which was made out of several parts of the DETCHEM toolbox, is coupled via an interface with OpenFOAM (programmed in C^{++}). For each cell, the variables pressure, gas temperature, wall temperature and concentrations of the gas phase species must be provided to the DETCHEM library by the CFD-code. Based on these values, the source terms of the gas-phase kinetics and of the surface reactions for the wall cells of catalytic coated surfaces are calculated using the library. These source terms are sent back to the CFD-code. The shared library also provides the properties heat conductivity, dynamic viscosity and the mixture-averaged diffusion coefficients of the gas phase species for every fluid cell to the CFD code. Additional details on the implementation of the mean-field approximation in DUO can be found in (Benzinger et al., 2019).

2.3. The Lattice-Boltzmann-method (LBM)

LBM is a numerical discretization scheme for Partial Differential Equations (PDEs) like the incompressible Navier-Stokes equation, which is based on mesoscopic models and described by kinetic equations, which are in turn linked to the targeted PDE (Krause, 2010). Further, the

fluid is regarded as a moving ensemble of particles (molecules) that are colliding and streaming. LBM can be viewed as coarse-graining of the molecular dynamics simulation where the fluid is literally presented by moving particles following Newtonian laws.

The fundamental variable in kinetic theory is the particle distribution function $f(\boldsymbol{x},\boldsymbol{\xi},t)$. It represents the density of particles with velocity $\boldsymbol{\xi}=\left(\xi_x,\xi_y,\xi_z\right)$ at position $\boldsymbol{x}$ and time t. However, the number of molecules is not constant in every direction. The spatial and temporal probability of movement of the fluid molecules into a direction i is described by the discrete distribution function $f_i(\xi)$ which is often called the particle population. This indicates the probability of finding a certain number of molecules which move into direction i.

Based on the quasi-Cartesian lattice, it is assumed that molecules starting from a node of a lattice can move only into a fixed number of Cartesian and diagonal directions to neighboring nodes. Along these directions the distribution functions f_i are streamed or moved, respectively. The lattice type chosen determines the count of directions. A velocity set for the LB algorithm is fully defined by two sets of quantities: the lattice velocities c_i and the corresponding weights w_i. In the code MATRICS the D2Q9 lattice is used (Fig. 2), where D is the dimension number, and Q is number of the nine discrete lattice directions i. Velocities and respective weights w_i are given in explicit form in Table 1.

The Boltzmann equation is a partial differential equation which describes the evolution of the populations in time (here written without any forces):

$$\frac{\partial f}{\partial t}+\xi_\beta \bullet \frac{\partial f}{\partial x_\beta}=\Omega(f)\alpha,\beta\in\{x,y\}\ . \tag{5}$$

This can be seen as a kind of advection equation: the first two terms represent the distribution function being advected with the velocity ξ of its particles. The source term on the right-hand side is the collision operator $\Omega(f)$, which represents the local redistribution of f due to collisions. By discretizing the Boltzmann equation in velocity, space and time the discretized Lattice Boltzmann equation can be derived:

$$f_i(x+c_i\delta t,t+\delta t)-f_i(x,t)=\Omega(f)=\frac{1}{\tau}\bullet\left(f_i^{eq}(x,t)-f_i(x,t)\right) \tag{6}$$

Again, the left hand side of this equation presents the convection (streaming) of the particle distributions, and the right hand side the collision term. As in most LBM codes in MATRICS the BGK (Bhatnagar Gross Krook) collision operator (Bhatnagar et al., 1954) is used.

When a gas has been left alone for sufficiently long time, one may assume that the distribution function $f_i(\boldsymbol{x},\boldsymbol{\xi},t)$ will reach an equilibrium distribution $f_i^{eq}(\boldsymbol{x},\boldsymbol{\xi},t)$. The discretized equilibrium distribution function derived from the Maxwell-Boltzmann equilibrium distribution is:

$$\boldsymbol{f_i^{eq}}(\boldsymbol{x},\boldsymbol{\xi},\boldsymbol{t})=\boldsymbol{w_i}\bullet\boldsymbol{\rho}\bullet\left(1+\frac{\boldsymbol{c_i}\bullet\boldsymbol{u_\alpha}}{\boldsymbol{c_s^2}}+\frac{(\boldsymbol{c_{i\alpha}c_{i\beta}}-\boldsymbol{c_s^2}\delta_{\alpha\beta})\bullet\boldsymbol{u_\alpha u_\beta}}{2\boldsymbol{c_s^4}}\right), \tag{7}$$

with $u_{\alpha\beta}$ as the local velocity components of the fluid (bulk motion). The relaxation time τ, from which the kinematic fluid viscosity υ can be derived, describes the time between two collisions of particles. In the BGK model the two parameters are connected according to

$$\upsilon=\left(\tau-\frac{1}{2}\right)\bullet c_s^2 \tag{8}$$

Table 1
D2Q9 velocity set in explicit form.

Directions i	Velocities directions c_i	Lengths $\lvert c_i\rvert$	Weights w_i
0	(0,0)	0	4/9
1, 2, 3, 4	(±1, 0), (0, ±1)	1	1/9
5, 6, 7, 8	(±1, ±1), (±1, ±1)	$\sqrt{2}$	1/36

The speed of sound which is $c_s=1/\sqrt{3}$ in lattice units can be derived from the D2Q9 velocity set. The solution algorithm of the LBM consists of only two steps: collision and streaming. In the first step the equilibrium and non-equilibrium distributions are calculated. These distributions are shifted to the neighbor cells in the streaming step.

2.3.1. The 2D LBM code MATRICS

The LBM code MATRICS (***MAT***thias + E***RIC*** + ***S***urface chemistry) works with the D2Q9 lattice. It allows the calculation of arbitrary shaped 2D regions implying detailed surface chemistry. The calculation of the chemical source terms is handled by connecting the toolbox DETCHEM^{TM} (Deutschmann et al., 2014) to the program MATRICS.

MATRICS offers features as solving an arbitrary number of species equations, importing and automatically meshing of files in PGM format for geometry description, restart capability, output in different formats (Paraview, Tecplot). The code is written in C++.

Up to now the density is constant, therefore only isothermal reactive flows with no change in mole numbers due to reactions can be calculated. However, the second constraint is fulfilled as a first approximation if temperature is constant and concentrations are small, which is the case in the actual work.

2.3.2. Implementation of species transport

The transport equation for a species a without any source term due to chemical reaction is

$$\frac{\partial C_a}{\partial t}+u\cdot\nabla C_a-\nabla(\rho\bullet D_a\bullet\nabla C_a)=0, \tag{9}$$

with C_a as the concentration (in [kmol/m^3]) and D_a as diffusion coefficient. In the framework of LB for every species a, a new discrete Lattice-Boltzmann equation based on populations $g_{a,i}$ is introduced:

$$g_{a,i}(x+\delta x,t+\delta t)-g_{a,i}(x,t)=\frac{1}{\tau_a}\bullet\left(g_{a,i}^{eq}(x,t)-g_{a,i}(x,t)\right) \tag{10}$$

g_a has the same unit as the concentration C_a (kmol/m^3). So far, this equation includes only streaming and collision. For the implementation of a chemical source term see section 2.3.2. The species equilibrium is defined with:

$$g_{a,i}^{eq}(x,\xi,t)=w_i\bullet C_a\bullet\left(1+\frac{c_i\bullet u_\alpha}{c_s^2}+\frac{(c_{i\alpha}c_{i\beta}-c_s^2\delta_{\alpha\beta})\bullet u_\alpha u_\beta}{2c_s^4}\right). \tag{11}$$

The relaxation time τ_a for each species is connected to the diffusion coefficient via the following relation:

$$D_a=\frac{\upsilon}{Sc_a}=\left(\tau_a-\frac{1}{2}\right)\bullet c_s^2 \tag{12}$$

with Sc_a as the Schmid number for each species. This model is a mass averaged version of the multicomponent LBM model for heterogeneous reactions from Sawant (Sawant and Karlin, 2025).

2.3.3. Implementation of chemical source terms

As described above the chemical source terms are calculated via a precompiled shared library. For each lattice touching a reactive wall the concentrations of the gas phase species and the temperature are send to the library and the source terms for all species are delivered back. As described above the source terms are defined in the unit of [mol/m^2/s)]. In principle, there are two possibilities to implement the source terms. Applying the sources as molar fluxes at the lattice interface to the wall or to reformulate the fluxes in analogy to homogeneous reactions as volumetric sources. Both approaches have been implemented and are described below.

2.4. Applying sources as wall fluxes (surface sources)

For explanation, it is asumed that the interface is aligned with the x-axis and that the transport domain is on the upper-hand side of the wall as shown in Fig. 3. In the example, the distribution functions g_4, g_7 and g_8 are streamed into the solid cells (in grey). After the collision step g_2, g_5 and g_6 come back from solid cells into fluid domain.

The method used for streaming back the populations is based on a mirror image scheme in which the boundary is seen as a mirror inside which all the cells in the domain see their images (Zhang et al., 2002). Hence, the missing populations for a boundary where a flux is imposed are deduced as:

$$\begin{aligned} g_{a,2}(t+\delta t) &= g^{*}_{a,4}(t) + \frac{4}{6}C_{a,source}, \\ g_{a,5}(t+\delta t) &= g^{*}_{a,8}(t) + \frac{1}{6}C_{a,source}, \\ g_{a,6}(t+\delta t) &= g^{*}_{a,7}(t) + \frac{1}{6}C_{a,\ source}, \end{aligned} \tag{13}$$

where $g^{*}_{a,i}$ are the post-collision populations. The mole flux $\dot{R}_{a,surface}$ of a species a per surface can be written as follows, where the effectiveness factor η_i is included in $F_{cat/geo}$ (compare Eq. (2)):

$$\dot{R}_{a,surface} = F_{cat/geo} \bullet \dot{s}_a in \left[\frac{kmol}{m^2 \bullet s}\right] \tag{14}$$

As the populations of the species g_i have the same unit as the concentrations C_a, the fluxes have to be converted into changes of concentrations. For this, we have to multiply by the physical interface area of the lattice $A_{interface} = \Delta x^2$, divide by the lattice volume $V_{lattice} = \Delta x^3$ and to multiply with the time step Δt. For the source in lattice units we get finally:

$$C_{a,source} = \dot{R}_{a,surface} \bullet \Delta x^2 \bullet \frac{\Delta t}{\Delta x^3} \bullet \frac{C_T}{C_L \bullet C_M} in \left[\frac{kmol}{m^3}\right] \tag{15}$$

C_L, C_T, C_M are the conversion factors for length, time and molar density (in [kmol/m^3]), respectively.

2.5. Applying sources as volumetric sources (volume sources)

As shown later, the usage of surface sources works very well in the case of straight surfaces which are either along x- or along y-direction. For these cases the geometrical surface is same as the surface of a lattice. However, if the geometrical interface is curved or skew and runs through a lattice, the change of single populations g_i is not straightforward. It is not clear how the fluxes should be distributed to the incoming populations. Therefore, it is nore sophisticated to incorporate the species fluxes at the interface as volumetric sources in the cell next to the interface. According this approach the source terms $C_{a,source}$ are directly implemented into the Boltzmann-Equation for the species and can be interpreted as additional force terms:

$$g_{a,i}(x+\delta x, t+\delta t) - g_{a,i}(x,t) = \frac{1}{\tau_a} \bullet \left(g^{eq}_{a,i}(x,t) - g_{a,i}(x,t)\right) + w_i \bullet C_{a,source} \tag{16}$$

This approach is accordingly to the one used from Sawant (Sawant and Karlin, 2025).

Typically, the total molar production rate (s˙_i) is obtained by solving the series of parallel Ordinary Differential Equations (ODE's) that describe the reaction rates (Eq. (1)). Solving the chemical source term in this way is also called direct integration and performed from the code DETCHEM (Deutschmann et al., 2014) which is coupled to MATRICS. The integration is done up to a certain physical time. For steady state calculations, like those shown in the present work, the end time for integration is set to 10 s. This means the chemistry is in quasi-steady equilibrium and we do not achieve an exact time dependent solution of the system. In such cases we can additionally strongly accelerate the calculation if we do not solve for reaction rates at every time step (e.g., here we solve reaction rates at only every 100th timestep). For time dependent solutions, however, we must set the integration time for chemistry to be the same size as the physical timestep and reaction rates must be solved at every timestep. In all scenarios, surface coverages must be stored after every calculation of reaction rates so that these values are available the next time reaction rates are evaluated.

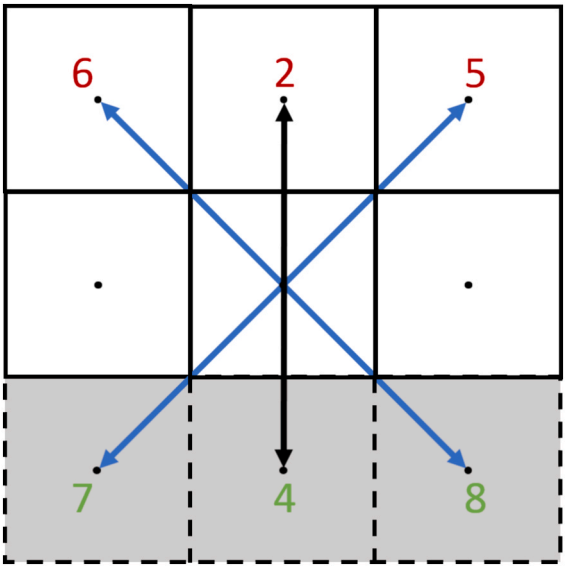

Fig. 3. Schematic illustration of the method for applying species fluxes at a wall. Lattices in grey belong to solid region.

3. Surface chemistry over a flat plate

The background of the experimental work is that CH_2O (formaldehyde) is formed as an intermediate species in the oxidation of methane and is thus present in the exhaust gas of lean-burned operating gas engines. In particular, high air–fuel ratios favor the formation of formaldehyde (Corrêa and Arbilla, 2005; Karavalakis et al., 2016; Lemel et al., 2005; Mitchell and Olsen, 1999; Yoon et al., 2014). Strict regulations for CH_2O emission with exhaust gas have been implemented. Therefore, there is a need to investigate conversion of CH_2O experimentally and through simulations.

3.1. Experimental methodology

Fig. 4 shows the calculation domain depicting the central part of the whole reactor system. The parallel wall channel has a height of 2 mm and a depth of 18 mm. An additional rectangular indentation is cut at the center of the bottom wall of the channel for placing the catalyst plate (length = 18 mm × width = 18 mm). The upper surface of the catalytic plate is positioned 400 μm lower than the ceramic bottom wall. The catalytic surface starts at x = 0 mm, and is located at y = -0.4 mm.

In the experiments (Wan et al., 2020), two-dimensional distributions of CH_2O (Formaldehyde) were measured with the PLIF (Planar Laser-Induced Fluorescence) technique. PLIF is a non-invasive laser-based

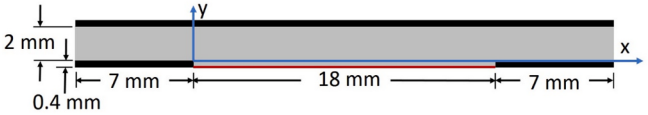

Fig. 4. Calculation domain.

technique which allows the visualization of the gas-phase species distributions at high spatial and – in case of using a single laser-shot – temporal resolution without disturbing the flow field. The top and side walls of the reactor are equipped with glass windows. The results are obtained for a slice in xy-plane which is positioned in the center of the reactor with respect to the z-axis (z = 9 mm).

Two different catalytic plates have been prepared which are coated with a catalyst-water slurry where the active component was platinum (Pt). To investigate the impact of catalyst loading, the slurry has been diluted by different dilution factors. The ratio of the catalytic surface area to geometric area $F_{cat/geo}$ (including the effectiveness factor η_i) was estimated to be 1 and 4, respectively. In (Wan et al., 2020) the measurement uncertainty of the concentration of CH_2O caused by the intensity deviation from single shots and the concentration fluctuation of the reference gas is within ± 20%.

3.2. Numerical setup

The same computational grid with rectangular cells was used in all cases and for both codes compared later. The number of grid points over the 18 mm long catalytic plate (red line in Fig. 4) was 360 in the streamwise direction, and includes a domain of 7 mm before and after the reaction zone, both discretized with 140 cells in axial direction. The height of the channel of 2 mm was discretized with 40 cells, the vertical distance between catalyst surface and channel bottom (40 μm) with 8 cells. In sum the equidistant grid consists of ca. 56,000 cells with a cell size of 50 μm.

The grid independency has been proven in preliminary simulations. All walls (black) are modeled as non-slip wall boundaries with the same wall-temperature as that measured in the experiments. The inlet (left) gas temperature is the same as the wall temperature for each case. The mass flow velocity at the inlet is determined according to the experimental conditions. Pressure outlet (right) into the atmosphere is employed as the outlet boundary.

In the validations, same operational conditions as in the experiments were used. A preheated gas mixture of 100–105 ppm CH_2O, 1.5 vol% H_2O, 5 vol% O_2, balanced with N_2, was fed into the reactor. Inlet temperature and the walls were set on same temperature of 373 K and 673 K, respectively (isothermal conditions).

3.3. Comparison of experiment and calculation

Fig. 5 shows the comparison of the measured (top) and calculated (bottom) mole fraction of CH_2O in the midplane slice of the channel.

The measured mole fractions in the midplane are shown on the top. The catalytic plate is marked in red. Due to restrictions in the experimental system not the whole cross section could be captured by the ICCD camera. The experiment shows that CH_2O is converted on the catalytic plate. The mole fraction decreases from 105 ppm at inlet to ca. 50 ppm at the outlet. There is a distinct gradient into vertical direction which proves that the system is controlled by mass transfer rather than by chemical kinetics.

The result of the calculation in the lower picture shows a good qualitative agreement with experimental data. The detailed comparison is shown in Fig. 6, where the mole fractions of CH_2O are compared on a line perpendicular to the catalytic plate at axial position of 12 mm (see red dashed line in Fig. 5). Two volume fluxes $\dot{V}$ of 0.5 and 1 $[ml/min]$ are compared.

The experiments reveal that the conversion increases with decreasing flowrate, as the velocity is smaller and, therefore, the residence time is longer. For both flowrates the system is under control of diffusion because the mole fraction of CH_2O is zero at the surface. The reaction is so fast that all CH_2O which is transported by diffusion to surface is converted.

The influence of the catalytic surface area $F_{cat/geo}$ at values 1 and 4 is

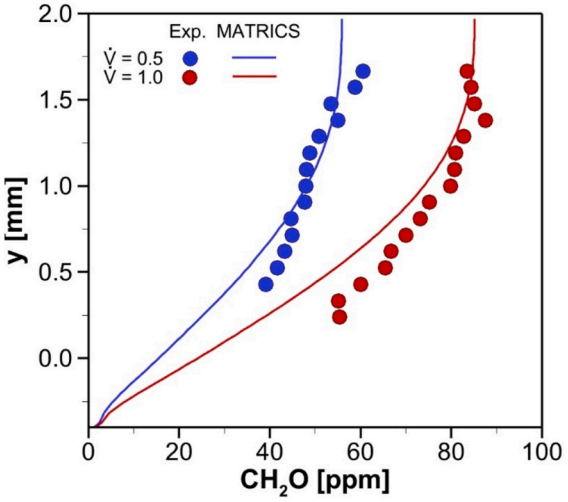

Fig. 6. Comparison of measured and calculated mole fractions of CH_2O perpendicular to catalytic plate at x = 12 mm from start of plate. Inlet concentrations and temperature are same as in Fig. 5 but now for two flowrates $\dot{V} = 0.5/1[ml/min]$.

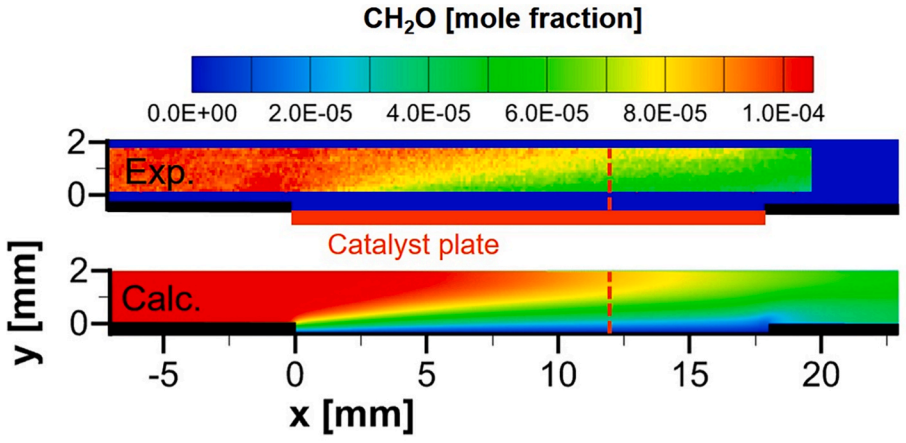

Fig. 5. Comparison of measured and calculated mole fractions of CH_2O in the midplane of the channel. Inlet conditions: volume flux at normal conditions $\dot{V} = 1[ml/min]$, temperature T = 673 K, $F_{cat/geo}$=4, mole fraction inlet $X_{CH2O} = 1.05 \cdot 10^{-4}$ (105 ppm). Flow is from left to right. The red dashed line marks the position for the slices shown in Figs. 6–8.

depicted in Fig. 7 for the temperature of T = 373 K and a volume flux of $\dot{V} = 1[ml/min]$. With respect to the calculations, the system is under kinetic control, at least for the smaller catalytic surface area of$F_{cat/geo} = 1$. Here, the reaction is too slow to convert all CH_2O which reaches the surface. Compared to the experimental data, it is evident that the conversion is overpredicted by the reaction mechanism for kinetically controlled conditions. It can be expected that the measured mole fractions on the catalytic surface at y = −0.4 mm are larger than those predicted by calculations.

As the focus of the paper is not to validate the reaction mechanism, further calculations have not been made. It should be noted that to validate the reaction mechanism experimental data are required at positions very close to the catalytic surface. But due to optical restrictions this was not the case in the experiments. The main conclusions drawn in this section would not change if not any experimental data would have been used for comparison. The main finding of these results is that the LBM code shows the same results as a finite volume approach.

The calculation with the codes MATRICS and DUO fit very well, which shows the capability of MATRICS for calculations of real systems with detailed surface chemistry.

The influence of the implementation approach for the chemical source terms as surface fluxes or volumetric sources (see section 2.3.2) is depicted in Fig. 8. It can be seen that the results for both approaches fit very well. In all following calculations, the volumetric source approach was used.

4. How to keep the exact geometrical surface

In the Mean-Field approach, the source terms for the species involved in surface chemistry are given in the unit [kmol/m^2/s^1]. The related area is defined as the geometrical area of the surface (Fig. 1). Therefore, it is essential that the geometrical surface used in calculation is the same as in reality.

For LBM grids, the surfaces of the cells, and therefore, also the interfaces between fluid and solid, are straight horizontal and vertical lines. The total surface of the staircase-shaped interface differs compared to the real surface and is in general wrong.

The code MATRICS is a 2D code. One of the topics objectives of this work is to help answer the question of how the exact *geometrical surface* of a body in a flow field can conserved to finally yield the exact species fluxes on the reactive surface of this body.

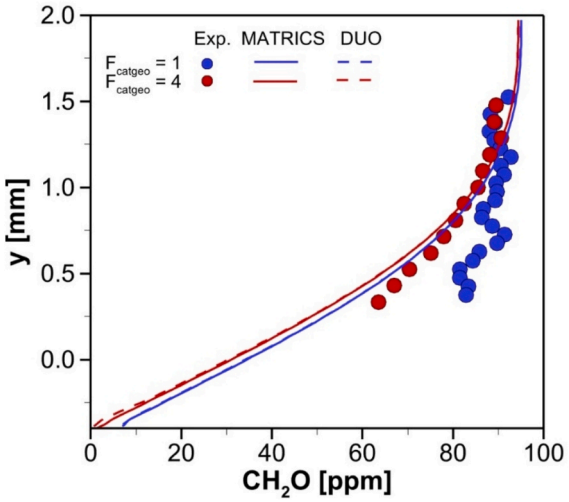

Fig. 7. Comparison of measured and calculated mole fractions of CH_2O perpendicular to catalytic plate at x = 12 mm. Inlet conditions: volume flux at normal conditions $\dot{V} = 1[ml/min]$, temperature T = 373 K, $F_{catgeo} = 1$ or 4, mole fraction inlet $X_{CH2O} = 1.0{\cdot}10^{-4}$ (100 ppm). Compared are experiments with results from the codes MATRICS and DUO.

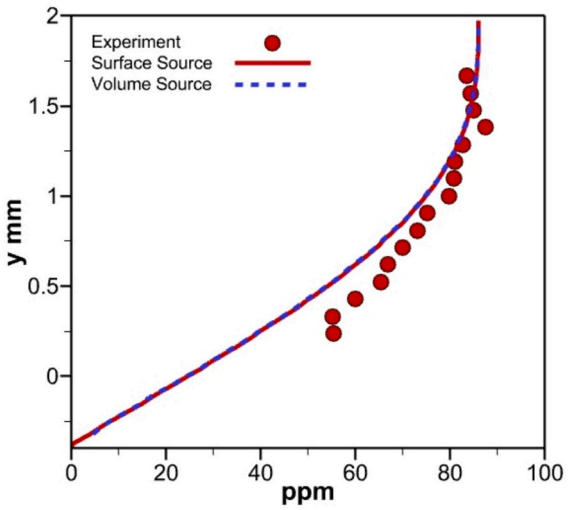

Fig. 8. Comparison of the two approaches for implementing the chemical $\dot{V} = 1[ml/min]$
Source terms into LBM (using surface fluxes or applying volumetric sources). Conditions are the same as for Fig. 6 ().

Firstly, the difference between the real geometric surface and the surface based on staircase-shaped interfaces will be quantified. Secondly, an approach will be shown where the exact surface in the calculations can be conserved if the geometry of the surface is known as a mathematical function. These two steps will be performed for both cylinders (circles) and prisms (squares).

For all calculation shown in this chapter, the simple generic kinetic mechanism for conversion of from species A to species B was used (see section 2.1.3).

4.1. Flow around circle with reactive surface

If we look at the flow around a cylinder in two dimensions, x and y, with infinite length in the z-direction, we identify the interface between cylinder and fluid as a circle. To keep things more intuitive, we analyze the length of this circle line (in 2D) rather than the surface of the cylinder (in 3D). Therefore, from now on, we refer to flow around a *circle* and not around a cylinder. The same holds for flow around *squares* and not around prisms with infinite length in the z-direction, which will be discussed later.

In the following, the discretization error of geometrical interface is quantified, and it is investigated whether the discretization error can be reduced with a finer resolution. We can examine the dependence on resolution in two different ways. On the one hand, we could hold the radius of the circle constant and increase the resolution of the grid (smaller cells). On the other hand, we can keep the lattice size constant and increase the radius of the circle. Here, the second approach will be used because the lattice size will be constantly kept equal to one and errors are only calculated as in normalized form.

4.1.1. Discretization error

The first question is how a circle, with a defined diameter, is discretized and how large is the deviation of the discretized staircase-shaped circumferential compared to the real circumferential. The ratio between the two values represents the error *E* incurred when using the staircase-shaped interface for calculation of species sources as opposed to the original interface.

Fig. 9 shows a lattice mesh. The lines represent the interfaces between the lattices. The center of each lattice is in the center of each square. The lattice size is $L_{lattice} = 1$.

The approach to discretize a circle is as follows. The circle center is

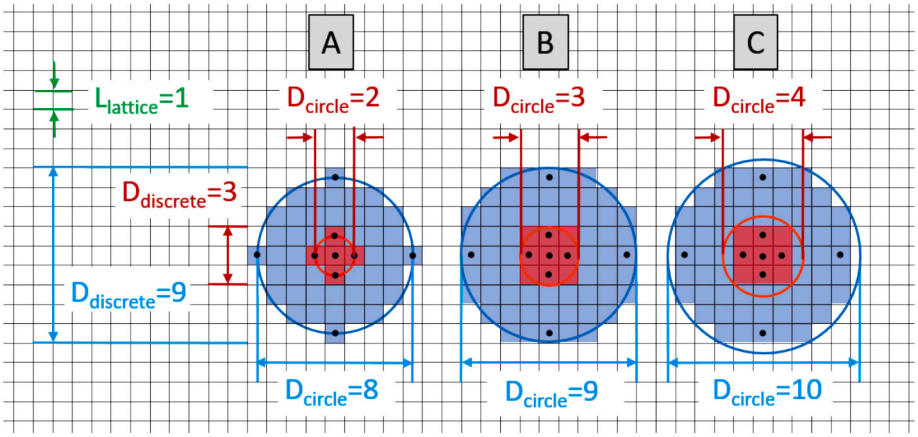

Fig. 9. Discretization of circles with different diameters. *Red* circles A/B/C with diameters D_{circle} = 2/3/4 have same discretized length of $L_{discrete}$ = 12. *Blue* circles A/B/C with diameters D_{circle} = 8/9/10 have same discretized length of $L_{discrete}$ = 36.

positioned in the center of a lattice cell. Then, all lattices whose cell centers have a distance to the circle center which is smaller or equal to the radius R of the circle are removed from the calculation domain and assigned to the solid domain.

First, we concentrate only on the blue circles. The corresponding solid or dead cells are marked in light blue in Fig. 9. For a circle with the diameter of D_{circle} = 8 we obtain the solid area as shown in Fig. 9A. The centers of the four outermost cell centers (black dots) lie directly on the circle and the related cells are therefore also removed. If we count the dead cells into x direction, we find that the dead region has the size of exactly $D_{discrete}$ = 9 cells in both directions.

For a circle with a diameter of D_{circle} = 9 the solid area shown in Fig. 9B results. The dead region has again the maximum size of $D_{discrete}$ = 9 cells into x- and y-direction. However more dead cells can be found.

For a circle with diameter D_{circle} = 10 minus a very small distance ε the resulting solid area is shown in Fig. 9C. It is the same as in Fig. 9B.

From now on, we assume that ε is very small. Meaning, we investigate circles with diameter from D_{circle} = 8 to D_{circle}≈10. All circles with diameter between 8 and 10 are discretized with a solid region with the size $D_{discrete}$ = 9.

If we sum up the staircase-shaped circumferential of each dead region (A, B or C) we get, in all three cases, the interface length of $L_{discrete}$ = 36. Fig. 10 serves as the explanation of this finding. In this figure the first two dead regions shown (A and B) are the same as shown in Fig. 9. Region D is a square with $D_{discrete}$ = 9. Additionally, a dead region E with equal extent in the x- and y-direction of $D_{discrete}$ = 9 is shown. All dead regions (A, B, D or E) show the same circumferential length of $L_{discrete}$ = 36.

For explanation we concentrate now on region E. Four cell corners with numbers from 1 to 4 are drawn which lie on a circle (not shown here). From each cell corner with a distinct number the cell corner with the following number can be reached by adding dead cells (in blue). However, "adding" of new blue cells must be done monotonically. That means, each following cell has to be *one step nearer* to the cell with next number either in the x- or y-direction. For the resolution chosen in this example, we have to step four cells into positive or negative x-direction and four cells into positive or negative y-direction from one of the corners to the next. The order of this stepping is not important. Finally, we always get nine cell surface lines between each pair of numbers summing up to $L_{discrete}$ = 4·9 = 36 for the whole solid region.

Now we calculate the error *E* we make if we discretize the blue circles in Fig. 9 with staircase-shaped interfaces. As stated before, the length of the discretized interface for circles with D_{circle} = 8 / 9 / 10 is equal to $L_{discrete}$ = 36. The error *E* in length is the ratio of discretized interface length $L_{discrete}$ over the real circle length:

$$E = \frac{L_{discrete}}{D_{circle} \bullet \pi}. \tag{17}$$

For the three blue circles with D_{circle} = 8 / 9 / 10 (blue cases A, B, C in Fig. 9) we get the values:

$$E_{blue,A} = \frac{36}{8 \bullet \pi} = 1.43; E_{blue,B} = \frac{36}{9 \bullet \pi} = 1.27; E_{blue,C} = \frac{36}{10 \bullet \pi} = 1.14. \tag{18}$$

This means that the discretization error *E* of interface length is between 14% and 43% depending on how large the circle diameter is in the range of D_{circle} = 8 to 10. So far, this result is only valid for the cases where we have circle with diameters leading to a dead domain with diameter of $D_{discrete}$ = 9.

Now, we perform the same analysis for the three red circles (red cases A, B, C,) in Fig. 9 with diameters D_{circle} = 2/3/4. The size of dead domain is $D_{discrete}$ = 3 and we get the following values for errors:

$$E_{red,A} = \frac{12}{2 \bullet \pi} = 1.9; E_{blue,B} = \frac{12}{3 \bullet \pi} = 1.27; E_{blue,C} = \frac{12}{4 \bullet \pi} = 0.95. \tag{19}$$

This means that the discretization error varies between an interface which is 90% too large or which is 5% too small depending on how large

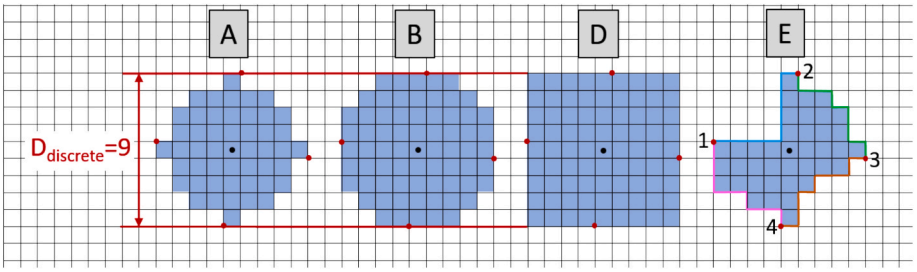

Fig. 10. Figures A/B/D/E with same discretized diameter $D_{discrete}$ = 9 have same interface lengths of $L_{discrete}$ = 36.

the circle diameter is in the range of $D_{circle} = 2$–4.

The next question to answer is, if the discretization error can be reduced with a finer resolution.

Therefore, we examine more circles. Fig. 11 shows ten circles where the diameter D_{circle} increases always by two cells. This is done for the conditions of circles of case B in Fig. 9. This means, that the extent of dead region is exactly the same as the circle diameter: $D_{circle} = D_{discrete}$. We start from the smallest circle (in grey) where the diameter is only discretized with one cell (in black). For this, the dead region shows 4 interface sides. The next circle with diameter of 3 cells has $4 + 8 = 12$ surface sides. For every increase of diameter by two additional lattices we get 8 new interface sides of the dead region. $D_{discrete}$ is labelled with a number for each circle shown. For example, the dead region for the light green circle ($D_{discrete} = 7$) has $L_{discrete} = 28$ interface sides, the brown one ($D_{discrete} = 9$) has $L_{discrete} = 36$ interface sides. It was shown above that a square has the same interface line length as the discretized dead region. Hence, the interface length is always:

$$L_{discrete} = 4 \bullet D_{discrete} \tag{20}$$

As we increase the discretization for every circle by 2 to get an uneven number of lattices per circle diameter, the number of additional interface sides is $8 = 4{\cdot}2$.

Above we performed the calculation of the error in interface lengths for cases A, B and C for distinct circle diameters from 2 to 4 (red circles) and from 8 to 10 (blue circles) (see Fig. 9). We seek now for formulas which describe the error E for arbitrary discretization $D_{discrete}$. The functions for the error E for each of the cases A/B/C are:

$$E_A = \frac{4 + i \bullet 8}{2i \bullet \pi}; E_B = \frac{4 + i \bullet 8}{(2i+1) \bullet \pi}; E_C = \frac{4 + i \bullet 8}{(2i+2) \bullet \pi}. \tag{21}$$

The index i goes from $i = 1$ to infinity. The resolution of a circle is $D_{discrete} = 2 \bullet i + 1$. We can see that for $i = 1$ we get $D_{discrete} = 3$ and the results shown above for red circles in Eq. (19). For i = 4 we get $D_{discrete} = 9$ and the results shown above for blue circle in Eq. (18). The plot of the three functions for $D_{discrete}$ up to 1000 is shown in Fig. 12.

We can see that for case B the error is independent from resolution E = 1.27. This is the ratio of the interface length of a square and a circle with same size and diameter:

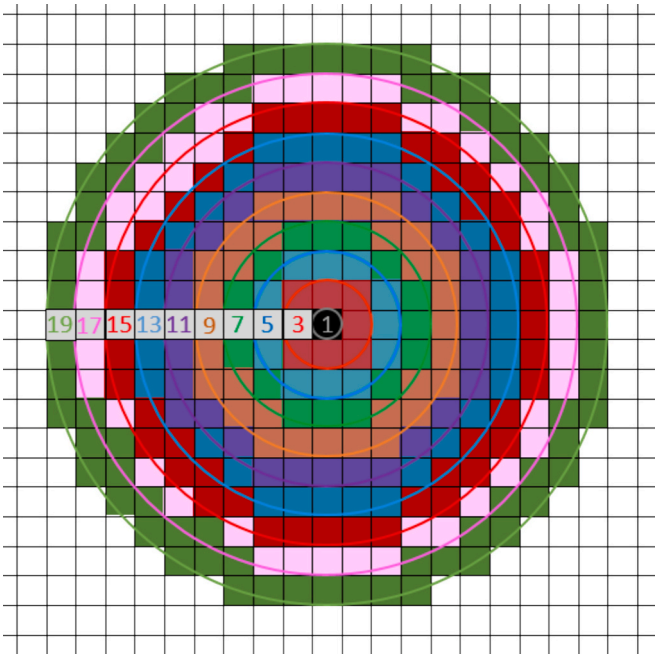

Fig. 11. Discretisation of circles with increasing resolution.

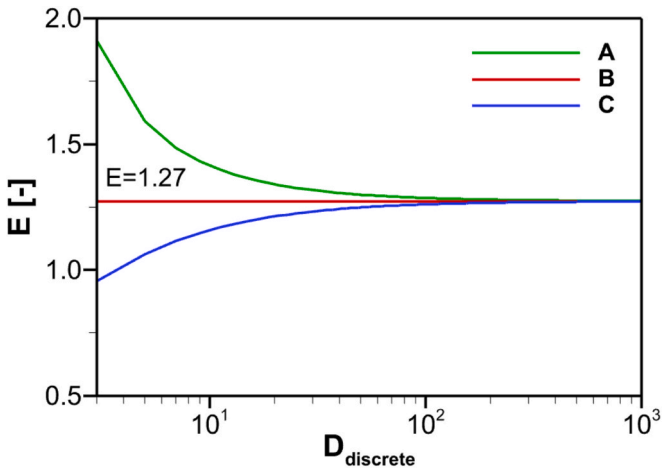

Fig. 12. Error of interface length for cases A/B/C of circle discretization.

$$E = \frac{L_{interface,square}}{L_{interface,circle}} = \frac{4 \bullet D_{discrete}}{D_{discrete} \bullet \pi} = \frac{4}{\pi} = 1.27. \tag{22}$$

For coarse discretization, the error is larger for cases A and smaller for cases C compared to cases B. This is because circles with slightly different diameter (in the range of two cell lengths) are discretized with same number of lattice cells. This is equal to the discretization error of the diameter itself. This also means that for increasing resolution the range of diameters of circles which are discretized with same cell count gets smaller because the discretization error of diemeter, which is two cells, decreases relative to cell diameter itself.

The error in interface length tends for both cases A and C towards the asymptotic value E = 1.27. This can also be deduced from the functions Eq. (21). The limiting value of the functions for $i \to \infty$ is in every case equal to 1.27.

$$\begin{aligned}
\lim_{i\to\infty} E_A\,(\mathrm{i}) &= \frac{4 + i \bullet 8}{2i \bullet \pi} \approx \frac{i \bullet 8}{2i \bullet \pi} = \frac{4}{\pi} = 1.27; \\
\lim_{i\to\infty} E_B\,(\mathrm{i}) &= \frac{4 + i \bullet 8}{(2i+1) \bullet \pi} = \frac{4 + i \bullet 8}{\pi + 2i \bullet \pi} \approx \frac{i \bullet 8}{2i \bullet \pi} = \frac{4}{\pi} = 1.27; \\
\lim_{i\to\infty} E_C\,(\mathrm{i}) &= \frac{4 + i \bullet 8}{(2i+2) \bullet \pi} = \frac{4 + i \bullet 8}{2\pi + 2i \bullet \pi} \approx \frac{i \bullet 8}{2i \bullet \pi} = \frac{4}{\pi} = 1.27.
\end{aligned} \tag{23}$$

This means, that if any circle is discretized with a not too coarse LBM grid, the staircase-shaped interface is 27% longer than the length of the circumferential of the original circle. Same holds for surface of an infinite cylinder in 3D.

The knowledge of this value offers users of codes where no surface correction is implied the possibility to correct the calculated conversion rates by factor 1.27 in case of flow around cylinders.

4.1.2. *Approach to use the exact geometrical surface*

The final approach of the reconstruction of the real surface length in the calculation is explained based on Fig. 13. For this approach we speak about *segmentation* of the staircase-shaped geometrical interface or using the ESC (Exact Surface Conservation) approach in the following.

We see a quarter of a circle and the resulting solid or dead domain as blue cells. All fluid cells which have an interface to the solid domain and where reaction takes place are marked in grey. The circle line crosses grey cells (fluid) and blue cells (solid). For calculation of the conversion rate in grey cells the length of the sections of the original circle in each of these cells are used as geometrical surface to calculate the local volumetric rate.

However, parts of the circle line lie within solid cells. Hence, these do not belong to any reactive cell. In the sketch, these sections are colored in red, purple and green. The line segments which belong to these cells

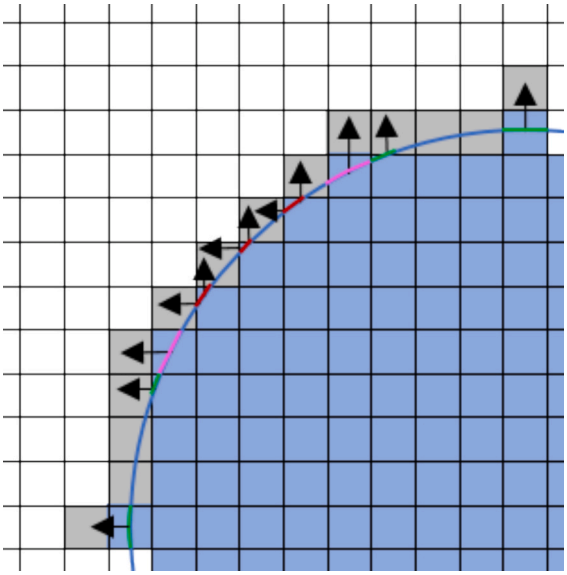

Fig. 13. Approach for segmentation of the geometrical interface.

are distributed into neighboring cells where reaction takes place (grey cells). The distribution of the line segments in dead cells to surrounding reactive fluid cells is done depending on the configuration of the cells in the neighborhood. If a dead cell is surrounded by two fluid corner cells the corresponding circle section is distributed equally to both corner cells (red line sections). If a dead cell with a line segment is surrounded from one corner cell and one normal wall cell, the line segment is added to the normal wall cell (purple line sections). If a dead cell is surround by only normal wall cells, the line segment is transferred to the normal wall cell (green line sections). By doing so, the exact length of the original circle and hence the exact surface is used in the calculation of the conversion rate.

The calculation and assignment of the line sections to reactive cells is done only once in the preprocessing step from the grid generator. The surface of each reactive cell is stored in a list which is read at start of calculation. For every cell where a surface rate is calculated, the surface source provided by DETCHEM is multiplied by the exact surface size stored. This single multiplication is negligible with respect to overall calculation time. The ESC approach is computationally very cheap and requires, compared to other methods, no interpolations of any field values. It can also be easily used for introducing heat fluxes at curvilinear walls or adapted to 3D codes.

The approach is fully compatible to handle simultaneously gas-phase chemistry. For these, the inclusion for reaction rates is also done via volumetric soucre terms. If we would find both surface chemistry and gas phase chemistry in wall cells this would only need the use of the sum of both volumetric sources to be applied for each gas phase species.

It was shown that the theoretical error in applying staircase-shaped surfaces does not depend on grid resolution. However, in the ESC approach another uncertainty comes into play. It can be seen in Fig. 13 that surface sections can be dedicated to neighboring wall cells in the fluid domain. This means that parts of the surface receive the reaction source term based on conditions in a cell which is next to the actual cell where the surface source is applied. As a result, the rate is calculated with gas-phase concentrations which are located not directly perpendicular to the surface section of interest. Errors of this type come into play for all methods where physical values are interpolated onto surfaces (e.g. immersed boundary method). This interpolation error is much smaller than the surface error itself and will indeed decrease with increasing resolution.

Presently we cannot handle arbitrary complex irregular shapes with the ESC algorithm, such as tomographic scans of porous bodies. For theses surfaces there is no mathematical description of the interface line available. The handling of irregular surfaces will be part of a future paper.

Techniques like immersed boundary method could in principle also be adapted to diminish the error in surface calculation because they also account for the physical surface and not the stair-case shaped surface. However, the nature of these methods is different. Namely, the aim of such methods is to interpolate flow variables onto the surface for the calculation of forces. Additionally, these techniques are more complicated to implement and are computationally more costly as they cannot be performed in a preprocessing step.

4.1.3. Results

The approach for using the exact geometrical surface is validated in the following. System is the flow in a channel around a circle (cylinder). The height of the channel is 0.08 m and the length is 0.12 m (see Fig. 14). Flow is from left to right. Reynolds number is 150, inlet velocity is 0.12 m/s m/s. As the Reynolds number is small and the calculation domain is relatively short there was no evidence for the occurrence of instabilities (Karman-Vortex-Street).

All the results in this chapter are shown for same resolution. The discretization of the inlet is 100. As axial length of channel is 1.5 times inlet height the total cell count is 100*150 = 15000. The circle has a diameter of 0.02 m (one quarter of the inlet size) and is therefore discretized with 25 lattices. Finer as well as coarser resolutions have been tested with the same exact results. The single step surface reaction (conversion of species A to B) was used in these cases because it was faster than using the detailed mechanism for lots of calculations which were performed. However, this does not restrict the findings discussed in the following in any direction.

Fig. 14 shows an isoplot of axial velocity u_x together with some streaklines. The flow is accelerated above and below of the obstacle and reaches values of approximately 0.23 m/s. The region which is confined by the white line is the recirculation zone (negative axial velocity). It ends at approximately x = 0.075 m.

By means of Fig. 15 the influence of surface segmentation for the calculations of source terms of the species equations is analyzed. The absolute sources in the reactive cells depend on the approach used to determine the interface lengths. The calculated mole fractions of species B (product species) using either the discretized interface are shown left or using the segmented interface (ESC approach) are shown right. The region shown is only a part of the whole calculation domain (compare Fig. 14). Additionally, the colors in the plots are not interpolated as

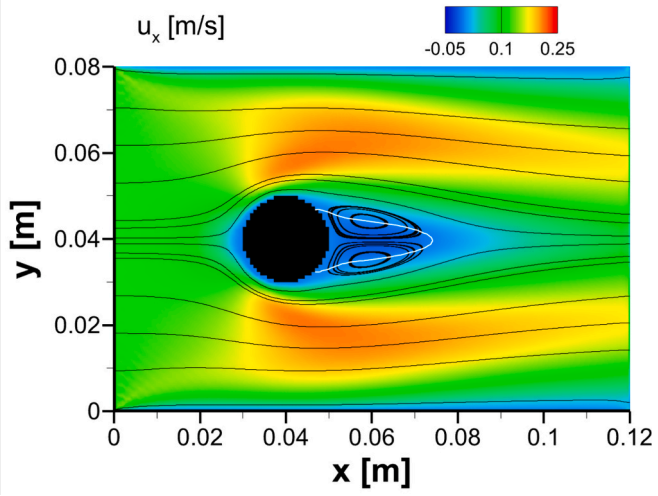

Fig. 14. Isoplot of axial velocity u_x together with some streaklines. The white line is the isoline of zero velocity and locates the recirculation zone. Resolution of circle is 25 lattices.

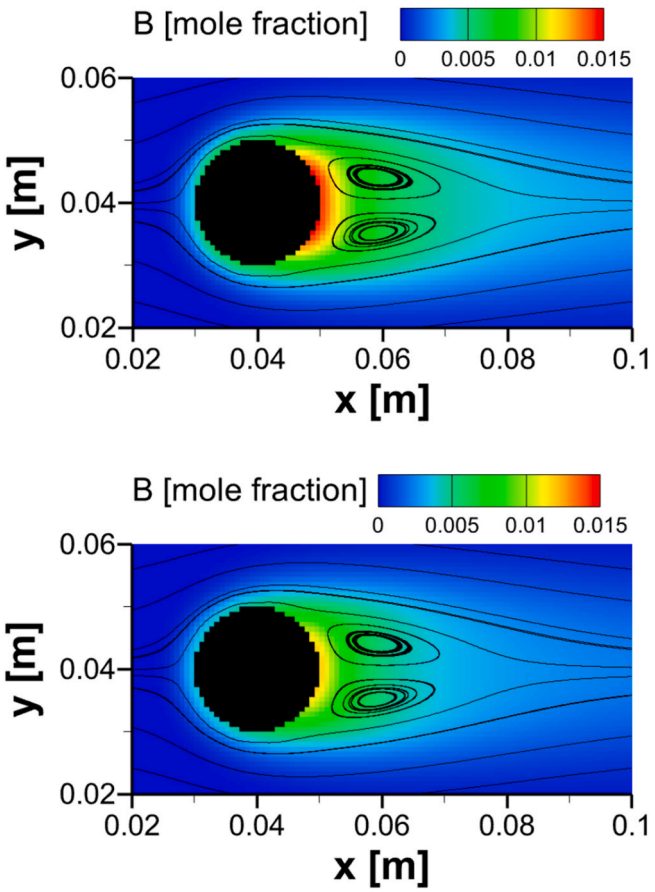

Fig. 15. Isoplot of molefraction of species B together with some streaklines. Top: calculation with staircase-shaped surface. Bottom: calculation with segmented interface. Resolution of circle is 25 lattices.

usually done (e. g. in Fig. 14). For each lattice cell we see a distinct color. This gives a direct impression of the resolution.

It can be clearly indicated that the mass for species B in the flow field is larger in the case of staircase-shaped interface (left) compared to the case using the segmented interface (right). As the surface is too large for the first case, the global conversion is too large. The rate in the first case is $1.43 \cdot 10^{-7}$ [kmol/s], in the second case $1.13 \cdot 10^{-7}$ [kmol/s]. The ratio of both values is 1.27 which is exactly the value predicted from theory (see Eq. (23)).

4.2. Flow around square with reactive surface

4.2.1. Discretisation error

For a flow around a prism with two equal side lengths in dimensions x and y with infinite length in the z-direction, we observe the interface between prism and fluid as a square. As in the case of circles we analyze perimeter of the square (in 2D) and not the surface area of the prism (in 3D).

A square consists of four skew perimeter lines. To quantify the discretization error for skew lines we start with a quarter of a circle with radius R = 1 in a xy-coordinate system (see Fig. 16). Center position of circle and starting position of any line is at origin. In the sketch, three example lines for three different angles α are shown. The end position of any line is on the circumference.

The length of each of these lines is R. Now, we investigate the discretized lines. We assume that all cell centers that are below and to the right of a line belong to solid material and all cell centers which are above and to the left or exactly on the line to the fluid material. Hence, the interface between the two phases is a staircase-shaped line.

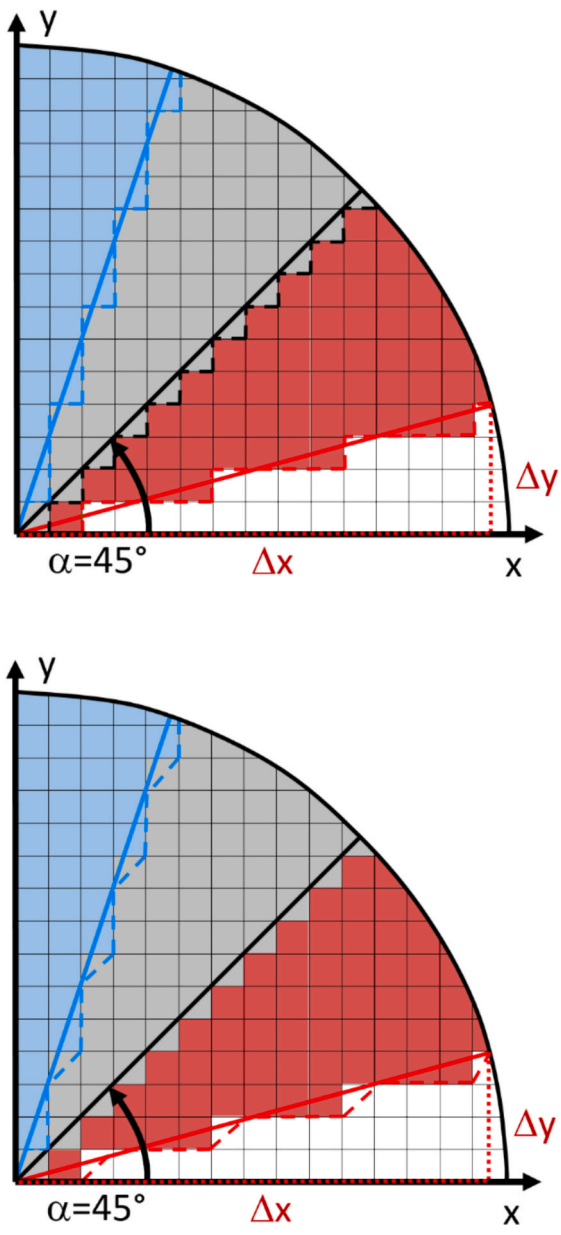

Fig. 16. Discretization of skew lines. Top: Interface is discretized with staircases. Bottom: beveled interface, line in cells with staircases is diagonal of cell.

Now we have a look closer look at the red line with the angle $\alpha = 20^\circ$. For the staircase holds:

- all horizontal cell sides sum up to the length $\Delta x = \cos(\alpha)$
- all vertical cell sides sum up to the length $\Delta y = \sin(\alpha)$

This holds for lines with an arbitrary angle. Finally, the length of the staircase-shaped intersection line (Fig. 16 left) is dependent on radius R and angle α and can be written as:

$$L_{\text{discretized}} = R \bullet (\cos(\alpha) + \sin(\alpha)). \tag{24}$$

The error of the discretization E as the ratio of the lengths of discretized line $L_{\text{discretized}}$ and real line $L_{\text{real}} = R$ is then:

$$E = \frac{L_{\text{discretized}}}{L_{\text{real}}} = \frac{R \bullet (\cos(\alpha) + \sin(\alpha))}{R} = \cos(\alpha) + \sin(\alpha) \tag{25}$$

Fig. 17 shows the error *E* as a function from angle α in the cases of lines

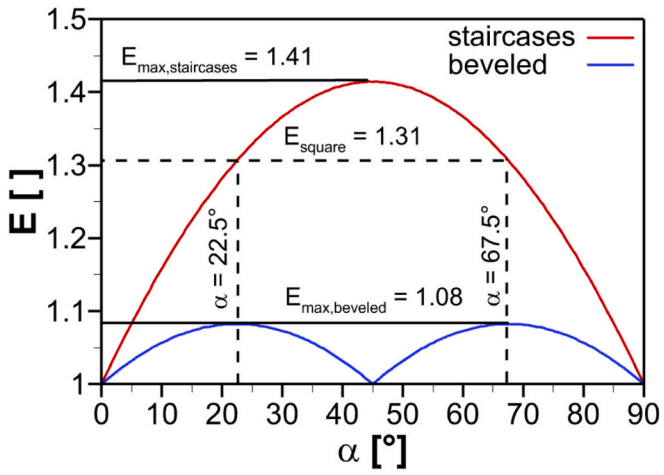

Fig. 17. Error for discretisation of skew lines depending on line angle. Red line: staircase-shaped interface. Blue line: beveled interface.

which are fully discretized with staircases. We can see that for horizontal and vertical lines the value E is equal to one, which implies that the discretized line has the same length as the real line. This is trivial because there are no staircases for the asymptotic cases of horizontal or vertical line. The angle $\alpha = 45°$ yields the maximum value of $E_{max,staircases} = \sqrt{2} = 1.41$, as the original length is that of the diagonal line.

In Fig. 17 additional results are shown if each staircase is discretized with the cell diagonal (see dashed lines in Fig. 16 right). It means for all staircases where the original interface length is 2 we reduce this length to $\sqrt{2}$. For this beveled interface line we can write:

$$\mathrm{E} = \frac{L_{\mathrm{discretized}}}{L_{\mathrm{real}}} = \cos(\alpha) + \sin(\alpha) + \min\left(\cos(\alpha),\ \sin(\alpha) \bullet \left(\sqrt{2} - 2\right)\right). \tag{26}$$

The blue line in Fig. 17 reveals that the maximum error for beveled lines $E_{max,beveled} = 1.08$ is for the angles $\alpha = 22.5°$ and $67.5°$ (see dashed lines in Fig. 17).

The consequences for an LBM code are as follows. A brute force approach to reduce the error in interface lengths for arbitrary geometries including curved or skew interfaces or where the real geometrical interface is not known as a mathematical function would be to replace the interface length of 2 lattice sides for any corner cells by the value of $\sqrt{2}$ (diagonal through lattice). By doing so, the global error in deducing the global surface of any geometry would be overpredicted by maximal 8.2% (if all interface lines are inclined by $\alpha = 22.5°$). The most simple implementation could be to multiply all rates in corner cells by the factor $1/1.082 = 0.93$.

Again, the knowledge of these values offer users of codes where no surface correction is implied, the possibility to correct the calculated conversion rates. As long as the angles of any inclined surfaces are known it is possible to multiply conversion rates for this surface by a factor which can be calculated from Eq. (25).

4.2.2. Approach to use the correct surface

The approach for reconstructing the real line length for arbitrary skewed lines is the same as previously shown for the circle case. All the rules for distributing the geometrical surface into reactive cells can be applied to other geometrical shapes as long as a mathematical function of the shape is available.

4.2.3. Results

Fig. 18 shows an isoplot of axial velocity u_x together with some streaklines for a flow around a square with size of 0.02 m which is rotated by 45° versus the x-axis. The center of the square is positioned at x = 0.04 m and y = 0.04 m, respectively. As the obstruction of the channel is a bit larger compared to the circle the maximum velocity is a bit larger and reaches now approximately 0.25 m/s. The recirculation zone (confined by the white line) is also larger in both directions. It ends axially at ca. x = 0.1 m.

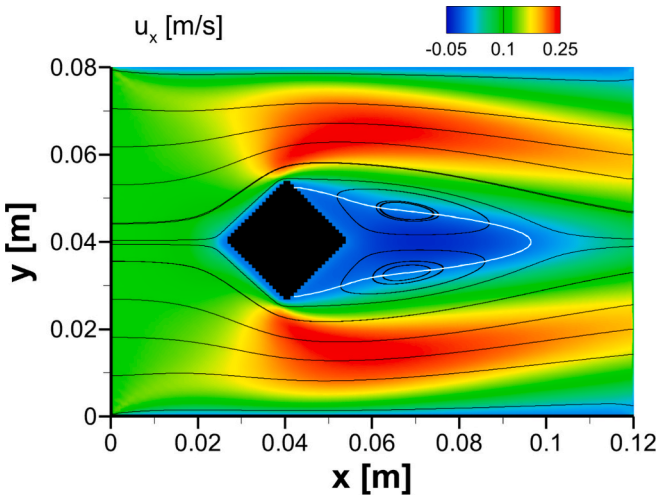

Fig. 18. Square with rotation angle of 45°. Isoplot of axial velocity u_x together with some streaklines. The white line is the isoline of zero velocity and locates the recirculation zone. Resolution of square is 25 lattices.

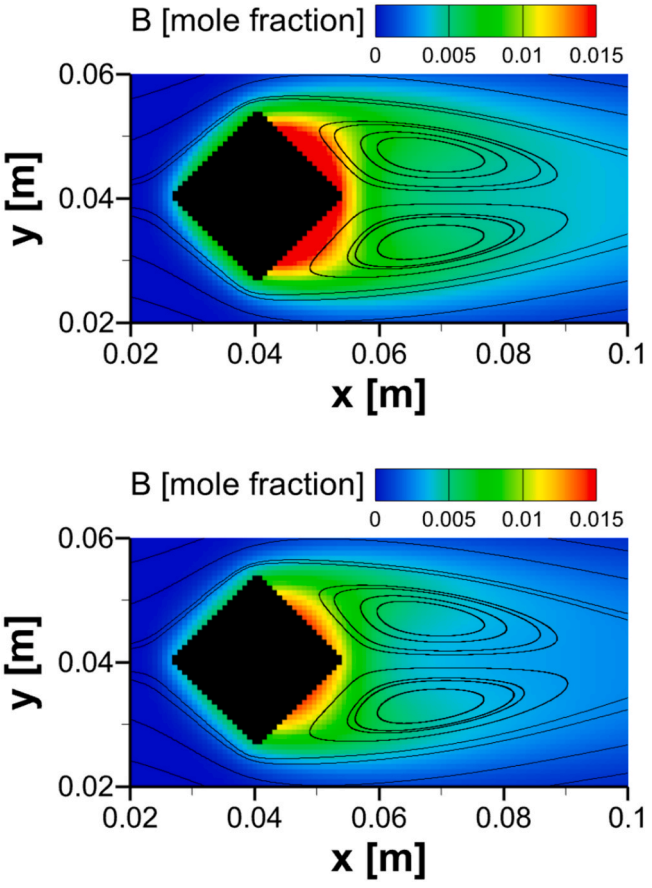

Fig. 19. Square with rotation angle of 45°. Isoplot of mole fraction of species B together with some streaklines. Top: calculation with staircase-shaped interface. Bottom: calculation with segmented interface. Resolution of square is 25 lattices.

In Fig. 19 we compare again the mole fraction of species B for the two approaches to handle the surface. The square consists of four skew lines which are inclined by 45° to the horizontal axis for which an error in line length/surface (and therefore also in global rate) of E = 1.41 is predicted (Eq. (25)).

As for the circle case, it can be seen that the mass for species B in the flow field is larger in the case of staircase-shaped interface (left) compared to the case using the segmented interface (right). The overall rate in the first case sums up to $1.95{\cdot}10^{-7}$ [kmol/s], in the second case it is $1.46{\cdot}10^{-7}$ [kmol/s]. The error E as ratio of both values is 1.38 which is slightly below the predicted value of 1.41. The reason is that the corners are not discretized with one cell only but with a plateau of 2 cells from the grid generation algorithm. Naturally, using a single spike cell is not possible. However, increasing resolution (diminishing influence of the corners) yields also the value of 1.41.

Finally, Fig. 20 shows an isoplot of axial velocity u_x together with some streaklines for a flow around a square with size of 0.02 m which is rotated by 22.5°. For this case the flow field is asymmetric and leads also to an asymmetric recirculation zone (confined by the white line) which ends axially at ca. x = 0.09 m.

On basis of Fig. 21 again the influence of the surface segmentation on the field of mole fraction of species B is analyzed. As expected also for this square the usage of staircase-shaped interface leads to too large mole fractions.

The actual square is defined by two boundary lines with angle of 22.5° and two lines with angle −67.5° (same skewness as a line with + 67.5°) with respect to x-coordinate. The error in surface for the lines with these two angles is the same and equals $E_{square} = 1.31$ (see dashed lines in Fig. 17). The calculated overall conversion rate in case of staircase-shaped interface (left) sums up to $1.83{\cdot}10^{-7}$ [kmol/s] compared to $1.42{\cdot}10^{-7}$ [kmol/s] for the case using the segmented interface (right). The error E as ratio of both values is 1.29 which is nearly the same as the theoretical value of 1.305.

It can be stated that the values for the error in surface for lines with angles + 22.5°, –22.5°, +67.5° and 67.5° are the same. This is because the value of E over angle is symmetrical to the angle of 45° and the function for E repeats for the other three quadrants of a Cartesian coordinate system.

Based on these findings we can conclude that the global error for the whole surface of a rotated square or a rectangle is the same than the error for any of the single lines of the body. This holds also for any other body which is confined only by straight lines which are orthogonal to each other.

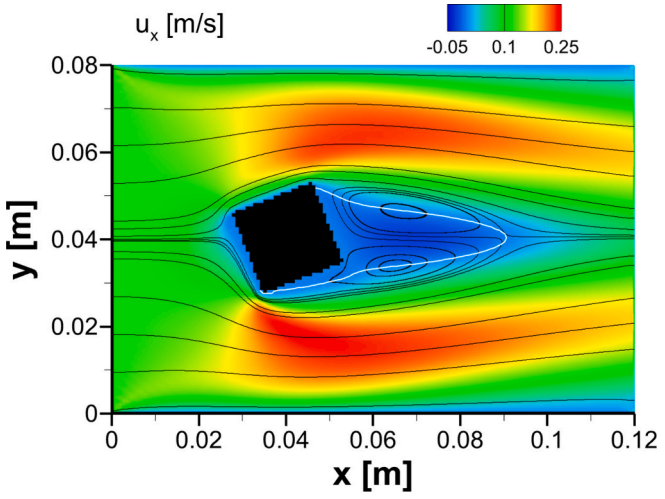

Fig. 20. Square with rotation angle of 22.5°. Isoplot of axial velocity u_x together with some streaklines. The white line is the isoline of zero velocity and locates the recirculation zone. Resolution of square is 25 lattices.

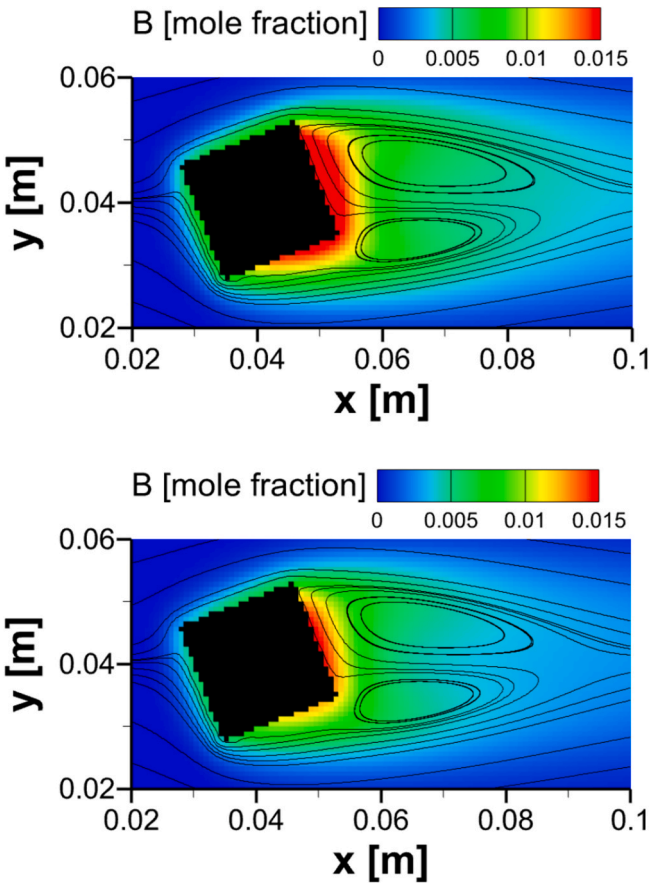

Fig. 21. Square with rotation angle of 22.5°. Isoplot of mole fraction of species B together with some streaklines. Top: calculation with staircase-shaped interface. Bottom: calculation with segmented interface. Resolution of square is 25 lattices.

5. Conclusions

This paper addresses the calculation of flow combined with detailed surface chemistry in 2D using the LBM code MATRICS. So far, the code is based on constant density. Species transport and detailed surface chemistry was added to the LBM framework.

Firstly, calculations of a reactor for catalytic conversion of formaldehyde were performed and the results compared with experimental data and results from the Finite-Volume-Method (FVM) code DUO. The results show good agreement with experimental data for operation conditions where the system is controlled by diffusion. However, it seems that the chemical mechanism used tends to overpredict the conversion for small temperatures or small catalytic activity (kinetically controlled system). However, the LBM results fit with the ones achieved from FVM code for all conditions.

As LBM works with Cartesian grids, the discretized interface between a solid body and the surrounding fluid is in general wrong. However, the exact geometrical surface of any catalyst must be considered in simulations including surface chemistry. The discretization error with respect to interface was quantified by means of theoretical considerations for 2D discretization of circles (infinite long cylinders in z-direction) as well as for skew lines (infinite long prims in z-direction).

The asymptotic error E for discretization of circles with increasing resolution is $E = \pi/4 = 1.27$. The discretization error of skew lines is dependent on angle α of the circumferential line to the x-axis. The error can be calculated using a simple formula and is maximal for an angle of $\alpha = 45^{\circ}$ ($E = \sqrt{2} = 1.41$). The knowledge of these values offers users of a code where no surface correction is implied the possibility to correct

the conversion rates for spherical or inclined surfaces.

Moreover, it can be stated, that the global discretization error for rotated squares, rectangles or any other bodies consisting of orthogonal boundary lines is the same as the error of any of the single inclined boundary lines of the body.

For inclined lines it was shown that the overall error is maximal 8% if the interface lengths of corner cells is set to the value of $\sqrt{2}$ (instead using the original length of two lattice sides). It was proven that the discretization error for curvilinear interfaces cannot be diminished by grid refinement.

An ESC (Exact Surface Conservation) approach was developed, which allows the use of exact geometric interface needed for considering surface reaction. In other methods the surface size is either not explicitly available or not exact. The approach consists of two steps.

(1) Implementation of the chemical conversion rates as sources into the LB equation. This is essential for a straightforward implementation of ESC approach. It was shown that the implementation of the chemical source terms as volumetric sources and not, as commonly done, as wall fluxes leads to same results
(2) Segmentation of the geometrical surface. In this step, the geometrical surface is distributed into reactive wall cells based on simple rules. This has to be done only once in a preprocessing step

The method was validated by calculation of flow around circles (cylinders) and squares (prisms) with different angles of rotation, all while considering a simple surface chemistry. The global conversion rates were compared between cases where the staircase-shaped surfaces were used compared to the cases where the segmented geometrical surfaces were used. The errors showed similar values to the ones predicted from theory.

This ESC approach is computationally very inexpensive and needs, compared to other methods, not any interpolations or extrapolations of field values. It does not influence stability and can also be used for heat flux calculation at curvilinear walls.

So far, the method is only developed and applied for 2D geometry. However, the principal approach can also be transformed and applied in 3D. This would need the segmentation of the geometrical surface into triangles like the algorithms used in the immersed boundary method (e.g. Marco Alacid et al., 2018). We would expect a negligible impact on overall calculation time also for a 3D code as the segmentation needs only to be done once during a preprocessing step.

CRediT authorship contribution statement

Matthias Hettel: Writing – original draft, Visualization, Validation, Software, Methodology, Investigation, Formal analysis, Data curation, Conceptualization. **Eric A. Daymo:** Writing – review & editing, Formal analysis. **Nilesh Sawant:** Formal analysis. **Olaf Deutschmann:** Resources.

Declaration of competing interest

The authors declare that they have no known competing financial interests or personal relationships that could have appeared to influence the work reported in this paper.

Acknowledgements

A cost-free academic license of DETCHEM™ by the omegadot Software & Consulting GmbH is gratefully acknowledged. We thank the Deutsche Forschungsgemeinschaft (DFG, German Research Foundation) for the financial support of project SFB 1441. Special thanks to Mrs. Romi Klöfer for fruitful discussions.

Data availability

Data will be made available on request.

References

T.K. Krüger, Halim Kuzmin, Alexandr Shardt, Orest , G. Silva, E.M. Viggen, The Lattice Boltzmann Method Principles and Practice, 1st 2017. ed.2017. doi: 10.1007/978-3-319-44649-3.

Hosseini, S.A., Boivin, P., Thévenin, D., Karlin, I., 2024. Lattice Boltzmann methods for combustion applications. Prog. Energy Combust. Sci. 102, 101140. https://doi.org/10.1016/j.pecs.2023.101140.

Kang, J., Prasianakis, N.I., Mantzaras, J., 2014. Thermal multicomponent lattice Boltzmann model for catalytic reactive flows. Phys. Rev. E 89, 063310. https://doi.org/10.1103/PhysRevE.89.063310.

Khatoonabadi, M., Prasianakis, N.I., Mantzaras, J., 2024. A pore-level 3D lattice Boltzmann simulation of mass transport and reaction in catalytic particles used for methane synthesis. Int. J. Heat Mass Transf. 221, 125025. https://doi.org/10.1016/j.ijheatmasstransfer.2023.125025.

Belot, I., Vidal, D., Greiner, R., Votsmeier, M., Hayes, R.E., Bertrand, F., 2021. Impact of washcoat distribution on the catalytic performance of gasoline particulate filters as predicted by lattice Boltzmann simulations. Chem. Eng. J. 406, 127040. https://doi.org/10.1016/j.cej.2020.127040.

N. Sawant, B. Dorschner, I. Karlin, Reactive mixtures with the lattice Boltzmann model, 2021. doi:10.48550/arXiv.2101.01702.

Sawant, N., Dorschner, B., Karlin, I., 2022. Consistent lattice Boltzmann model for reactive mixtures. J. Fluid Mech. 941, A62. https://doi.org/10.1017/jfm.2022.345.

D.G.M. Goodwin, Harry K. Schoegl, Ingmar , R.L.W. Speth, Bryan W. , Cantera: An object-oriented software toolkit for chemical kinetics, thermodynamics, and transport processes (Version 3.1.0), (2024). doi:10.5281/zenodo.14455267.

Filippova, O., Hänel, D., 2000. A novel lattice BGK approach for low mach number combustion. J. Comput. Phys. 158, 139–160. https://doi.org/10.1006/jcph.1999.6405.

Arcidiacono, S., Mantzaras, J., Karlin, I.V., 2008. Lattice Boltzmann simulation of catalytic reactions. Phys. Rev. E 78, 046711. https://doi.org/10.1103/PhysRevE.78.046711.

Succi, S., Smith, G., Kaxiras, E., 2002. Lattice Boltzmann simulation of reactive microflows over catalytic surfaces. J. Stat. Phys. 107, 343–366. https://doi.org/10.1023/A:1014531209244.

Li, X., Cai, J., Xin, F., Huai, X., Guo, J., 2013. Lattice Boltzmann simulation of endothermal catalytic reaction in catalyst porous media. Appl. Therm. Eng. 50, 1194–1200. https://doi.org/10.1016/j.applthermaleng.2012.08.058.

Ginzburg, I., d'Humières, D., 2003. Multireflection boundary conditions for lattice Boltzmann models. Phys. Rev. E 68, 066614. https://doi.org/10.1103/PhysRevE.68.066614.

Bouzidi, M., Firdaouss, M., Lallemand, P., 2001. Momentum transfer of a Boltzmann-lattice fluid with boundaries. Phys. Fluids 13, 3452–3459. https://doi.org/10.1063/1.1399290.

Noble, D.R., Torczynski, J.R., 1998. A Lattice-Boltzmann method for partially saturated computational cells. Int. J. Modern Phys. C (IJMPC) 09, 1189–1201.

Filippova, O., Hänel, D., 1998. Grid Refinement for Lattice-BGK Models. J. Comput. Phys. 147, 219–228. https://doi.org/10.1006/jcph.1998.6089.

G. Falcucci, Chapter Two - LBM for 2D and 3D chemical reactors, in: H.E.A. Van den Akker (Ed.) Advances in Chemical Engineering, Academic Press2020, pp. 81-141. doi:10.1016/bs.ache.2020.04.004.

Yoshida, H., Nagaoka, M., 2010. Multiple-relaxation-time lattice Boltzmann model for the convection and anisotropic diffusion equation. J. Comput. Phys. 229, 7774–7795. https://doi.org/10.1016/j.jcp.2010.06.037.

Verhaeghe, F., Arnout, S., Blanpain, B., Wollants, P., 2006. Lattice-Boltzmann modeling of dissolution phenomena. Phys. Rev. E 73, 036316. https://doi.org/10.1103/PhysRevE.73.036316.

R.J. Kee, M.E. Coltrin, P. Glarborg, Chemically Reacting Flow, Wiley-Interscience2003.

Deutschmann, O., 2011. Modeling and simulation of Heterogeneous Catalytic Reactions: from the molecular process to the technical system. Wiley-VCH Weinheim.

Hettel, M., Wörner, M., Deutschmann, O., 2018. Computational fluid dynamics of catalytic reactors. In: Andreoni, W., Yip, S. (Eds.), Handbook of Materials Modeling: Applications: Current and Emerging Materials. Springer International Publishing, Cham, pp. 1–34. https://doi.org/10.1007/978-3-319-50257-1_6-1.

Torkashvand, B., Maier, L., Lott, P., Schedlbauer, T., Grunwaldt, J.-D., Deutschmann, O., 2019. Formaldehyde oxidation over platinum: on the kinetics relevant to exhaust conditions of lean-burn natural gas engines. Top. Catal. 62, 206–213. https://doi.org/10.1007/s11244-018-1087-y.

OpenFOAM-The Open Source CFD Toolbox, www.openfoam.org, 2017.

O. Deutschmann, S. Tischer, C. Correa, D. Chatterjee, S. Kleditzsch, V.M. Janardhanan, N. Mladenov, H.D. Minh, H. Karadeniz, M. Hettel, DETCHEM Software package, www.detchem.com, Karlsruhe, Germany, 2014.

M. Hettel, C. Diehm, H. Bonart, O. Deutschmann, Numerical simulation of a structured catalytic methane reformer by DUO: The new computational interface for OpenFOAM® and DETCHEM™, Catalysis Today, 258 (2015) 230-240.http://doi.org/10.1016/j.cattod.2015.02.011.

Hettel, M., Daymo, E., Deutschmann, O., 2018. 3D modeling of a CPOX-reformer including detailed chemistry and radiation effects with DUO. Comput. Chem. Eng. 109, 166–178. https://doi.org/10.1016/j.compchemeng.2017.11.005.

Benzinger, W., Daymo, E., Hettel, M., Maier, L., Antinori, C., Pfeifer, P., Deutschmann, O., 2019. Reverse water gas shift (RWGS) over Ni – Spatially-resolved measurements and simulations. Chem. Eng. J. 362, 430–441. https://doi.org/10.1016/j.cej.2019.01.038.

M.J. Krause, Fluid Flow Simulation and Optimisation with Lattice Boltzmann Methods on High Performance Computers - Application to the Human Respiratory System, Karlsruhe Institute of Technology (KIT), 2010. doi:10.5445/IR/1000019768.

Bhatnagar, P.L., Gross, E.P., Krook, M., 1954. A model for collision processes in gases. I. Small amplitude processes in charged and neutral one-component systems. Phys. Rev. 94, 511–525. https://doi.org/10.1103/PhysRev.94.511.

Sawant, N., Karlin, I.V., 2025. Mean field lattice Boltzmann model for reactive mixtures in porous media. J. Fluid Mech. 1011, A9. https://doi.org/10.1017/jfm.2025.359.

Zhang, X., Crawford, J.W., Glyn Bengough, A., Young, I.M., 2002. On boundary conditions in the lattice Boltzmann model for advection and anisotropic dispersion equation. Adv. Water Resour. 25, 601–609. https://doi.org/10.1016/S0309-1708(02)00027-1.

Corrêa, S.M., Arbilla, G., 2005. Formaldehyde and acetaldehyde associated with the use of natural gas as a fuel for light vehicles. Atmos. Environ. 39, 4513–4518. https://doi.org/10.1016/j.atmosenv.2005.03.042.

Karavalakis, G., Hajbabaei, M., Jiang, Y., Yang, J., Johnson, K.C., Cocker, D.R., Durbin, T.D., 2016. Regulated, greenhouse gas, and particulate emissions from lean-burn and stoichiometric natural gas heavy-duty vehicles on different fuel compositions. Fuel 175, 146–156. https://doi.org/10.1016/j.fuel.2016.02.034.

Lemel, M., Hultqvist, A., Vressner, A., Nordgren, H., Persson, H.K., Johansson, B., 2005. quantification of the formaldehyde emissions from different HCCI engines running on a range of fuels. SAE Trans. 114, 1347–1357.

Mitchell, C.E., Olsen, D.B., 1999. Formaldehyde formation in large bore natural gas engines part 1: formation mechanisms. J. Eng. Gas Turbines Power 122, 603–610. https://doi.org/10.1115/1.1290585.

Yoon, S., Hu, S., Kado, N.Y., Thiruvengadam, A., Collins, J.F., Gautam, M., Herner, J.D., Ayala, A., 2014. Chemical and toxicological properties of emissions from CNG transit buses equipped with three-way catalysts compared to lean-burn engines and oxidation catalyst technologies. Atmos. Environ. 83, 220–228. https://doi.org/10.1016/j.atmosenv.2013.11.003.

Wan, S., Torkashvand, B., Häber, T., Suntz, R., Deutschmann, O., 2020. Investigation of HCHO catalytic oxidation over platinum using planar laser-induced fluorescence. Appl. Catal., B 264, 118473. https://doi.org/10.1016/j.apcatb.2019.118473.

O. Marco Alacid, J. Ródenas, F. Fuenmayor, M. Tur, An extension of shape sensitivity analysis to an immersed boundary method based on Cartesian grids, Computational Mechanics, 62 (2018).10.1007/s00466-017-1522-0.